DNA-based Nanoconstructs for the Detection of Ions and Biomolecules with Related Raman/SERS Signature Studies

BY

KIMBER L. BRENNEMAN
B.S., Purdue University, 2003

THESIS

Submitted as partial fulfillment of the requirements
for the degree of Doctor of Philosophy in Bioengineering
in the Graduate College of the
University of Illinois at Chicago, 2013

Chicago, Illinois

Defense Committee:

Michael A. Stroscio, Chair and Advisor
Mitra Dutta, Co-Advisor, Electrical & Computer Engineering
Michael Cho
G. Ali Mansoori
Thomas L. Theis, Environmental Science and Policy

TABLE OF CONTENTS

LIST OF FIGURES & TABLES

LIST OF ABBREVIATIONS

QD	Quantum Dot
FRET	Fluorescence Resonant Energy Transfer
Hg	Mercury
Pb	Lead
mRNA	Messenger Ribonucleic Acid
Cd	Cadmium
SNP	Single Nucleotide Polymophisms
CRP	C-reactive Protein
SPR	Surface Plasmon Resonance
PL	Photoluminescence
SELEX	Systematic Evolution of Ligands by Exponential Enrichment
SERS	Surface-enhanced Raman Scattering/Spectroscopy
AgFON	Silver Film Over Nanospheres
AgNR	Silver Nanorod
OAD	Oblique Angle Deposition
NP	Nanoparticles
BLL	Blood Lead Levels
OSHA	Occupational Safety and Health Association
WHO	World Health Organization
nt	Nucleotide
PCR	Polymerase Chain Reaction
NC	Nanocrystals
LED	Light Emitting Diodes
EDC	1-Ethyl-3-[3-dimethylamino propyl]carbodiimide Hydrochloride
Sulfo-NHS	N-hydroxysulfosuccinimide
AuNP	Gold Nanoparticle
FRET	Fluorescence Resonant Energy Transfer
NSET	Nanometal Surface Energy Transfer
DABCYL	4-([4-(dimethylamino)phenyl]azo) benzoic acid
MW	Molecular Weight
UV	Ultra Violet
TCEP	Tris(2carboxyethyl)phosphine
EDTA	ethylenediamine tetraethyl acetate
MWCO	Molecular Weight Cut Off
PBS	Phosphate Buffered Saline

SUMMARY

The utilization of DNA aptamers and semiconductor quantum dots (QDs) for the detection of ions and biomolecules was investigated. In recent years, there have been many studies based on the use of DNA and RNA aptamers, which are single stranded oligonucleotides capable of binding to biomolecules, other molecules, and ions. In many of these cases, the conformational changes of these DNA and RNA aptamers are suitable to use fluorescence resonant energy transfer (FRET) or nanometal surface energy transfer (NSET) techniques to detect such analytes. Coupled with this growth in such uses of aptamers, there has been an expanded use of semiconductor quantum dots as brighter, longer-lasting alternatives to fluorescent dyes in labeling and detection techniques of interest in biomedicine and environmental monitoring. Thrombin binding aptamer (TBA) and a zinc aptamer were used to detect mercury, lead, zinc, and cadmium. These probes were tested in a liquid assay as well as on a filter paper coupon.

Biomolecules were also studied and detected using surface-enhanced Raman spectroscopy (SERS), including DNA aptamers and C-reactive protein (CRP). Raman spectroscopy is a useful tool for sensor development, label-free

detection, and has the potential for remote sensing. Raman spectra provide information on the vibrational modes or phonons, between and within molecules. Therefore, unique spectral fingerprints for single molecules can be obtained. SERS is accomplished through the use of substrates with nanometer scale geometries made of metals with many free electrons, such as silver, gold, or copper. In this research silver SERS substrates were used to study the SERS signature of biomolecules that typically produce very weak Raman signals.

1 INTRODUCTION

1.1 Background

The topic of this research is the utilization of aptamers and semiconductor quantum dots (QD) for the detection and monitoring of ions and biomolecules. In recent years, there have been many studies based on the use of DNA and RNA aptamers that bind to biomolecules, other molecules, and ions. In many of these cases, the conformational changes of these DNA and RNA aptamers are suitable to use fluorescence resonant energy transfer (FRET) and electron transfer (electron donor) techniques to detect the indicated analytes --- biomolecules, other molecules, and ions. As will be discussed in this document, such single-molecule and single-ion detection techniques have enormous potential in biomedical applications ranging from laboratory research to portable self-administered tests, as well as environmental testing of toxins and exposure effects. Indeed, in this document, the use of aptamers to detect analytes in human saliva will be discussed in some detail (1-10). Coupled with this growth in such uses of aptamers, there has been an expanded use of semiconductor quantum dots as brighter, longer-lasting alternatives to fluorescent dyes in labeling and detection techniques of interest in biomedicine (11-21).

1.2 Motivation

The detection of toxic heavy metal ions in biological fluids or environmental samples is useful in determining human exposure levels and if that exposure is going to be damaging. Mercury (Hg) exposure, which can cause neurological problems, is mainly from fish consumption and possibly dental amalgams (22). Lead (Pb) is also an extremely toxic heavy metal ion worth monitoring. Detection of potential toxins in the environment and in biological samples such as urine, blood, or saliva that can be done in a fast and inexpensive manner would have great value. In the case of highly toxic heavy metals, detection at low concentrations would be necessary. In addition to testing biological media for toxins, biomarkers that are related to toxicity could also be measured to determine early signs of toxicity before any permanent damage occurs. Metallothioneins for example, are a family of proteins in humans produced in response to heavy metal exposure (23). The protein itself could potentially be measured with an aptamer, however a simpler biomarker would be the transcript or the sequence of mRNA which could be done using a molecular beacon (24). In fact, metallothionein mRNA in peripheral blood lymphocytes is considered a biomarker for cadmium (Cd) exposure (25). Moreover, single

nucleotide polymorphisms (SNPs) in genes can also be detected with molecular beacons. A SNP in the metallothionein gene 2A has been studied by McElroy *et al*. (26) and it is possible that this SNP could be a contributor to the variability of cadmium concentrations in tissues. All of these biomarkers are extremely well suited to detection with DNA-based QD nanosensors.

Moreover, there are indications that cancer biomarkers in saliva, especially mRNA, (27) may be detected using these aptamer-based nanosensors. In addition, there is some prospect of using known aptamers to detect C-reactive protein (CRP), which is a biomarker for inflammation and cardiovascular disease (28). A 44-base RNA aptamer has been selected for CRP and has demonstrated CRP sensing with surface plasmon resonance (SPR) (29). A DNA aptamer that is 72 bases long has also been selected (30).

Other possible analyte candidates for detection using these nanosensors are: (a) anthrax biomarker calcium dipicolinate, which is a component of the anthrax spore (31); (b) β_2-microglobulin and retinol binding protein as cadmium exposure biomarkers; and (c) alpha-glutathione S-transferase levels in urine has

been shown to correlate with the early stages of nephrotoxicity due to lead exposure (32).

Finally, as will be discussed, these nanosensors may be used to detect ions of interest such as mercury, lead, zinc, and cadmium (33, 34). Toxicity from the heavy metal ions lead (Pb), mercury (Hg), and cadmium (Cd) can all result in renal dysfunction (35). While zinc is an ion required for normal physiological function, it can also result in toxicity upon excessive supplementation (36). Toxicity from the heavy metal lead (Pb) can adversely affect several organs and body systems and potentially cause cardiovascular disease, hypertension, renal dysfunction, Autism and Parkinson's disease. Determination of lead exposure can be done through measurement of blood, urine and bone Pb levels. These species are biomarkers for lead poisoning. Blood-Pb is an indicator for recent or acute exposure and urine-Pb levels provide information on the body burden over a longer period of exposure. The bone-Pb level tells what the body burden dose was from Pb over the lifetime of exposure. An independent study shows high risk of cardiovascular disease for individuals with a Blood Lead Level (BLL) < 5 μg/dL. 15% of Pb exposed workers had BLL above OSHA (Occupational Safety

and Health Association) permissible limits. In another independent study of lead mobilization test on children, multiple positive correlations were found between the severity of autism and the urinary excretion of toxic metals. WHO and OSHA safety level for Pb are 1.45 µM (30 µg/dL) and 1.93 µM (40 µg/dL) respectively (37). Above these safety levels concentration of lead in the body can be toxic.

Concentrated mercury poses serious problems to human health, as bioaccumulation of mercury within the brain and kidneys ultimately leads to neurological diseases. To control mercury pollution and reduce mercury damage to human health, sensitive determination of mercury is important (22). The concentration of mercury in drinking-water sources is usually less than 0.5 µg/liter, but sometimes groundwater can have higher concentrations. Many studies involving the observation of more than 1000 individuals indicate that the classical signs and symptoms of elemental mercury vapor poisoning (objective tremors, mental disturbances and gingivitis) may be expected to appear after chronic exposure to air mercury concentrations above 0.1 mg/m^3 (38). Ingestion of 500 mg of mercury (II) chloride causes severe poisoning and sometimes death in humans. Acute effects result from the inhalation of air containing mercury

vapor at concentrations in the range of 0.05–0.35 mg/m^3. Exposure for a few hours to 1–3 mg/m^3 may give rise to pulmonary irritation and destruction of lung tissue and occasionally to central nervous system disorders (38). Among the high consumers of fish, the median concentrations of mercury were 8.6 µg/L in blood, 2.4 µg/g in hair, 10 pg/L in end-exhaled air, and 1.1 µg/g creatine in urine. The relationship between freshwater fish consumption and mercury was significant in all biological media. The high-consumption group had much higher mercury levels in blood (9-fold), hair (7-fold), alveolar air (3-fold), and urine (15-fold) than the low-consumption group (39).

Cadmium is a contemporary metal with many industrial uses, and cadmium emissions to the atmospheric, aquatic, and terrestrial environment have increased over the years (40). The kidneys are usually the most critically affected organs in occupational exposure to Cd; known to adversely interfere with the renal handling of plasma derived proteins. Tubular proteinuria should also be considered as an adverse effect attributed to Cd exposure, because it can lead to irreversible renal damage associated with an exacerbation of the age-related decline in glomerular filtration rate and a decrease in the filtration reserve

capacity. The biological exposure thresholds for controlling health significant nephrotoxic effects in adults occupationally exposed to Pb and/or Cd are 700 µg Pb/L in blood and 5 µg Cd/L in blood (32). The table below summarizes the toxic effects of the metals discussed.

Heavy Metal	Sources of Exposure	Toxicity Levels	Toxicity Effects
Lead (Pb)	Occupational, drinking water	WHO: <1.45 uM (30 ug/dL) OSHA: <1.93 uM (40 ug/dL)	Cardiovascular disease, hypertension, renal dysfunction, Autism, Parkinson's disease
Mercury (Hg)	Fish, drinking water, dental amalgams	OSHA: <0.1 mg/m^3 (time weighted avg.) EPA: max. contamination level for drinking water is 2ug/L (10 nM)	Cardiovascular disease, renal dysfunction, Autism
Zinc (Zn)	Supplementation (RDA is 15 mg/day)	100-300 mg Zn/d associated with toxicity	Copper deficiency, neutrapenia, anemia, adverse effect on ratio of LDL/HDL cholesterol
Cadmium (Cd)	Occupational, Cigarette smoke; food/ drink	OSHA: 5 mg/m^3 ACGIH: Threshold Limit Values are 10 $\mu g/m^3$ total, 2 $\mu g/m^3$ inhalable fraction	Renal dysfunction, proteinuria, hepatotoxicity

Table 1: Summary of heavy metals detected using DNA-based nanosensors.

As a final example, of the potential uses of these nanosensors, it is noted that they are potentially well suited for detecting biomarkers in saliva, where concentrations are typically much lower than serum (41).

In developing these aptamer-based nanosensors it is essential to have methods of assessing the success of synthesis techniques as well as measuring physical signatures corresponding to specific nanostructures and biomolecules. Optical techniques such as Raman scattering and photoluminescence (PL) are widely appreciated as potent tools for the study of the optical, electronic, and vibrational (thermal) properties of materials including those relevant to these studies including: semiconductor nanostructures such as quantum dots; biomolecules including DNA, RNA, and aptamers; and nano-complexes based on constructs that incorporate both semiconductor nanostructures and biomolecules. Moreover, surface-enhanced Raman scattering (SERS) provides a map of the vibration modes of a nanostructure or a biomolecule that may be used in assessing the success of synthesis techniques as well as measuring physical signatures corresponding to specific nanostructures and biomolecules. In this study, techniques for advancing the state-of-the-art in the use of these

optical tools will be explored to facilitate the step-by-step diagnosis and analysis of the nanoconstructs being fabricated for biomedical applications such as detection of ions and biomolecules using potentially self-administered tests. SERS-related techniques will be given a high priority in the cases where SERS-active structures can be successfully designed. Progress in the use of SERS is illustrated by the fabrication of SERS substrates using silver (42-44). Moreover, SERS has been considered as a possible basis for chemical and biological nanosensors (45). Furthermore, the fundamental role played by plasmons in the SERS process has been considered by a number of authors including Ref. (46). Techniques for enhancing Raman signals through substrate fabrication include: (a) nanosphere lithography to produce a silver film over nanospheres (AgFON) (47), (b) silver nanorod (AgNR) arrays fabricated with the Oblique Angle Deposition (OAD) technique at University of Georgia –Athens (42) and used to detect trace levels of viruses by Shanmukh et al. 2006 (48), (c) optical antennas (49), (d) metal doped sol-gels (50), and (e) gold core with silver shell nanoparticles (NP) (51, 52).

The long term goals of this research are to develop a sensitive and selective sensor for biomedical testing that are rapid, low-cost and have the ability to be integrated into a portable hand-held device or used by individuals without special training or as self-diagnostic tests. The use of aptamers and QDs as a detection platform along with the advantages of SERS allows for many possibilities for detecting toxins, pathogens, and different types of biomarkers, including proteomic and transcriptomic (mRNA) markers in the environment and in biological fluids, especially saliva. Additionally, the study of Raman signatures for important biomarkers and toxins will contribute to the body of knowledge of specific molecular signatures. This will help further efforts in biosensing techniques which are label-free, non-invasive, and potentially remote (53).

1.3 Objectives

In this document, a research program using both aptamers and semiconductor quantum dots and Raman spectroscopy for biomedical applications and environmental testing will be investigated. Specifically, the following research topics will be explored: ion and biomolecule detection using aptamer-based optical nanoconstructs; the optimization of synthesis parameters

for optical aptamer-based probes, fabrication of surface enhanced Raman scattering (SERS) substrates using silver; and SERS signatures of selected biomolecules. The detection schemes investigated in this study will be used as a platform for the design of a portable hand-held device or for point of care diagnostics.

1.3.1 Design, fabrication, and testing of DNA aptamer-based ion detection assays for integration into a portable handheld testing device.

1.3.2 Advancing techniques for using Raman and PL analyses for the study of: (a) DNA aptamers (DNA in nano-complexes used as probes for single-biomolecule and single-ion detection) (b) analytes (including C-reactive protein).

1.3.3 Design of DNA aptamer-based nano-complexes for optical detection of analytes in saliva.

2 NANOMATERIALS

There has been a large increase over the past decade in the development of nanomaterials and their applications in sensors. These nanomaterials can be used as building blocks in the design of nanosensors for the detection of a vast range of analytes and various signal transduction methods.

2.1 DNA Aptamers

Aptamers are single stranded DNA or RNA molecules that have an affinity for certain targets, which can include metal ions, small molecules, nucleic acids, proteins, and even complex structures such as cells. This binding capacity is based on the tertiary structure of the folded sequence. DNA is typically more stable than RNA, however modifications can be made to RNA aptamers to improve robustness. Aptamers are also easily conjugated to nanomaterials via functional groups such as carboxyls or amines or dithiols. Oligonucleotides have been used as molecular recognition elements in a broad range of detection schemes and targets. Molecular beacons are hybridization probes that detect particular sequences of single stranded DNA. These probes have enough

specificity to distinguish between two strands of DNA with only one differing nucleotide as a result of their stem-loop structure (24).

2.1.1 SELEX – Aptamer Synthesis

SELEX or the systematic evolution of ligands by exponential enrichment was initially described in 1990 by Ellington and Szostack as well as by Tuerk and Gold (54, 55). This chemical process has fewer limitations than the biological selection process used for creating antibodies. Furthermore, an aptamer can be selected for toxic compounds, such as heavy metals because they are selected for through an *in vitro* chemical process, whereas antibodies are created using an *in vivo* biological process (56).

SELEX involves the selection of relatively short nucleotide (nt) sequences from large libraries (10^{15}) of single stranded DNA or RNA. The basic steps of the SELEX process are described below, but there are many variations, as it can be tailored for specific requirements. The starting pool of random oligonucleotide sequences is chemically synthesized. Also, the range of targets for aptamers is quite varied including peptides, proteins, carbohydrates, whole cells and small

molecules like metal ions and the smallest identified ethaneolamine. The five-step process used in iterative rounds is described here (57):

1. Binding – target is incubated with random pool; the random sequences are typically 20-80 nucleotides with a constant region on either end (18-21 nt), which contains primer binding sites needed for polymerase chain reaction (PCR) in the amplification step.
2. Partition – target immobilization on matrix material or in affinity chromatography column or with magnetic beads; ultra filtration based on molecular weights with nitrocellulose paper is also used to separation without immobilization
3. Elution – the bound oligonucleotides are eluted for further processing
4. Amplification – enrich selected pool with PCR and attach functional groups for detection, immobilization and enlargement
5. Conditioning – dsDNA from previous step has to be either transcribed into ssRNA or separated into ssDNA for the next round

Once the affinity of the selected oligonucleotides cannot be increased more, the selection process is over and cloning and characterization are

performed. This usually occurs after 6-20 rounds. The number of different sequences that are cloned can vary greatly but is very often in the neighborhood of 50 or more. These aptamers are then sequenced and analyzed so sections that are involved in target binding can be identified as they are usually reoccurring segments among the final pool of aptamers. Another important part of aptamer synthesis is post-SELEX modification. These modifications are made in order to improve stability, increase binding ability, and/or allow for detection or immobilization in applications. Several modifications made to confer nuclease resistance include substituting the 2'-OH on the ribose with a 2'-F or 2'-NH_2 or 2'-O-methyl, 3'-end capping with streptavidin-biotin or an inverted thymidine, and 5'-end capping. Sequence truncation is also done to remove segments not involved in target binding. An additional selection round is often required to ensure that target affinity was maintained.

2.1.2 Aptamer Structure

The primary structure of DNA is the specific sequence of nucleobases, Guanine (G), Cytosine (C), Adenine (A), and Thymine (T). This is what is responsible for our genetic information and in that case a double-stranded helix

forms the tertiary structure. In the case of DNA aptamers and RNA, which are single-stranded, the tertiary structure as a result of base pairing can result in motifs such as stem-loops, pseudoknots, or G-quartets. These tertiary structures are what determine the binding characteristics of aptamers. The conformation of an aptamer can be analyzed using a program like *mfold*, which was created by Zuker and can be found online at (http://www.bioinfo.rpi.edu/applications/mfold/dna/form1.cgi) (58). *Mfold* predicts the folding of nucleic acids by way of an energy minimizing algorithm and takes into account stems, loops, and bulges.

2.1.3 Aptamers versus Antibodies

Aptamers interact with analytes in a manner similar to antibodies. However, the ability of aptamers to detect small molecules makes their applications more diverse than antibodies. This broad range of targets gives aptamers an advantage over antibodies, which bind with protein targets. Moreover, aptamers have the capability of being selected for toxic targets, such as heavy metal ions, due to the chemical synthesis process.

	Aptamers	Antibodies
Affinity	Low nM-pM	Low nM-pM
Specificity	High	High
Production	In vitro chemical process	In vivo biological system
Target range	Wide: ions, small organic molecules, proteins, whole cells, etc.	Narrow: only immunogenic compounds
Batch to batch variation	Little or no	Significant
Chemical modification	Easy & straightforward	Limited
Thermal denaturation	Reversible	Irreversible
Shelf-life	Unlimited	Limited

Table 2. Comparison of aptamers to antibodies.

2.2 Semiconductor Quantum Dots

Semiconductor nanocrystals (NC) or quantum dots (QD) are often used in optical nanosensors where the photogenerated fluorescence is generally enhanced or decreased (33, 59). Quantum dots are spherical nanocrystals composed of semiconductors with size tunable optical and electronic properties. These inorganic nanocrystals are similar to organic fluorophores, in that they emit light upon excitation by a higher energy light source. However, QDs have several advantages compared to organic dyes (60, 61) including 1) a broad

excitation range which allows one light source to be used for a range of emission wavelengths, 2) narrow, symmetric, and tunable emission peak allowing multiplexing (62) and 3) they are more stable at higher temperatures and less prone to photobleaching. CdSe quantum dots coated with a thin layer of ZnS have quantum yields of 50%, which is quite high (63). These materials also produce semiconductor nanocrystals that emit in the visible range like the PL shown in Figure 1 for QDs that emit red light. This property is useful for imaging and biosensing applications.

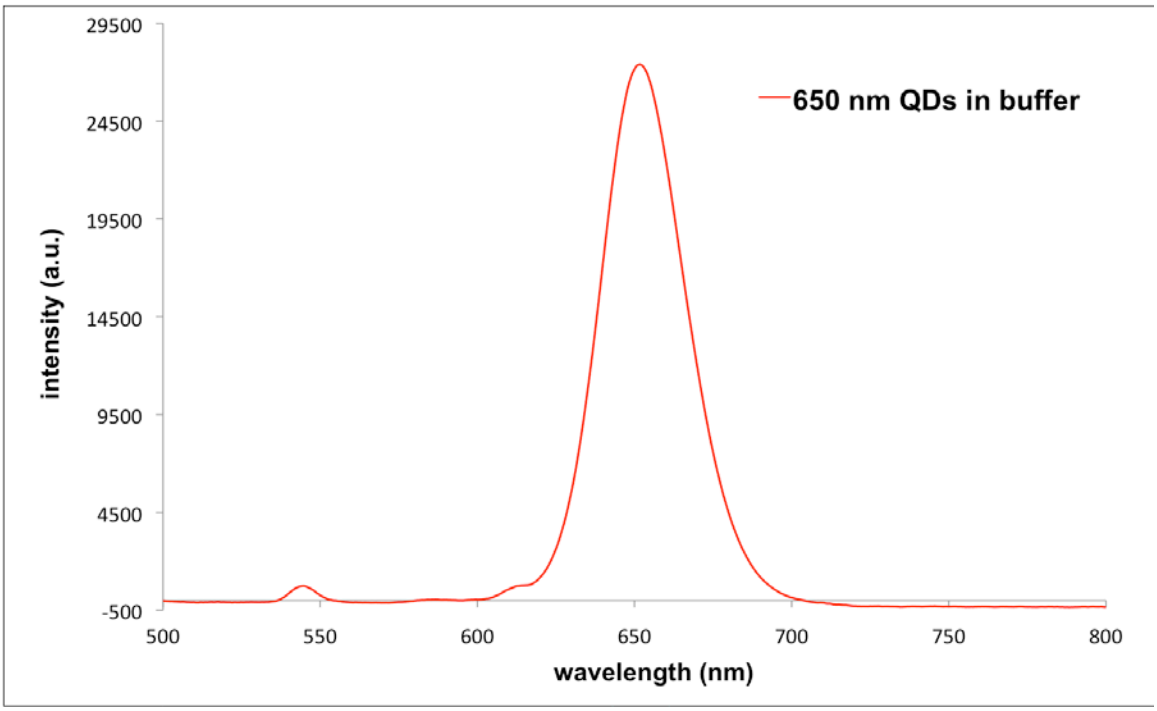

Figure 1. Photoluminescence spectrum of 650 nm CdSe/ZnS core/shell QDs in Tris-acetate buffer at concentration 10 nM.

Quantum dots have special properties due to their nanoscale dimensions. When excited by a source with higher energy than the emission wavelength, the electrons in the conduction band are kicked up to the valence band. Once these electrons recombine with the holes left in the conduction band, photons are emitted with a wavelength that is dependent upon the size of the band gap energy of the nanocrystal. For example, the excitation source for the QD emission in Figure 1 is a 380-nm light emitting diode (LED). Therefore, the same material can be used to fabricate quantum dots that emit at different wavelengths.

Quantum dots are functionalized in order to form nanoconstructs for sensing applications. Quantum dots used in biological assays must also have a coating to make it miscible in aqueous solutions (64). In order to bind QDs to biological molecules, such as DNA, they must be functionalized with a chemical moiety like carboxyl groups or amine groups. These functional groups will form covalent bonds with appropriately modified ligands, like nucleic acids. For example, QDs coated with carboxyl groups will bind to reactive amines, which can be found on proteins or as a functional group on the terminus of DNA. These

bonds are formed with the use of cross-linkers like EDC (1-Ethyl-3-[3-dimethylamino propyl] carbodiimide Hydrochloride) and Sulfo-NHS (N-hydroxysulfosuccinimide). In this work carboxyl-functionalized QDs will be used for optical signal transduction through conjugation to DNA aptamers.

2.3 Gold Nanoparticles

Gold nanoparticles (AuNP) are used in this research as quenchers or acceptors. A quencher absorbs energy from a donor molecule, such as a QD or an organic fluorophore. This energy transfer phenomenon is known as Fluorescence Resonant Energy Transfer (FRET). AuNPs absorb a much broader range of visible light than organic quenchers such as Iowa Black FQ, which absorbs light between 420 – 620 nm. The UV/VIS absorption spectrum of the Nanogold product that was used in this research is shown in Figure 2, as provided by Nanoprobes Inc. It covers the entire visible spectrum.

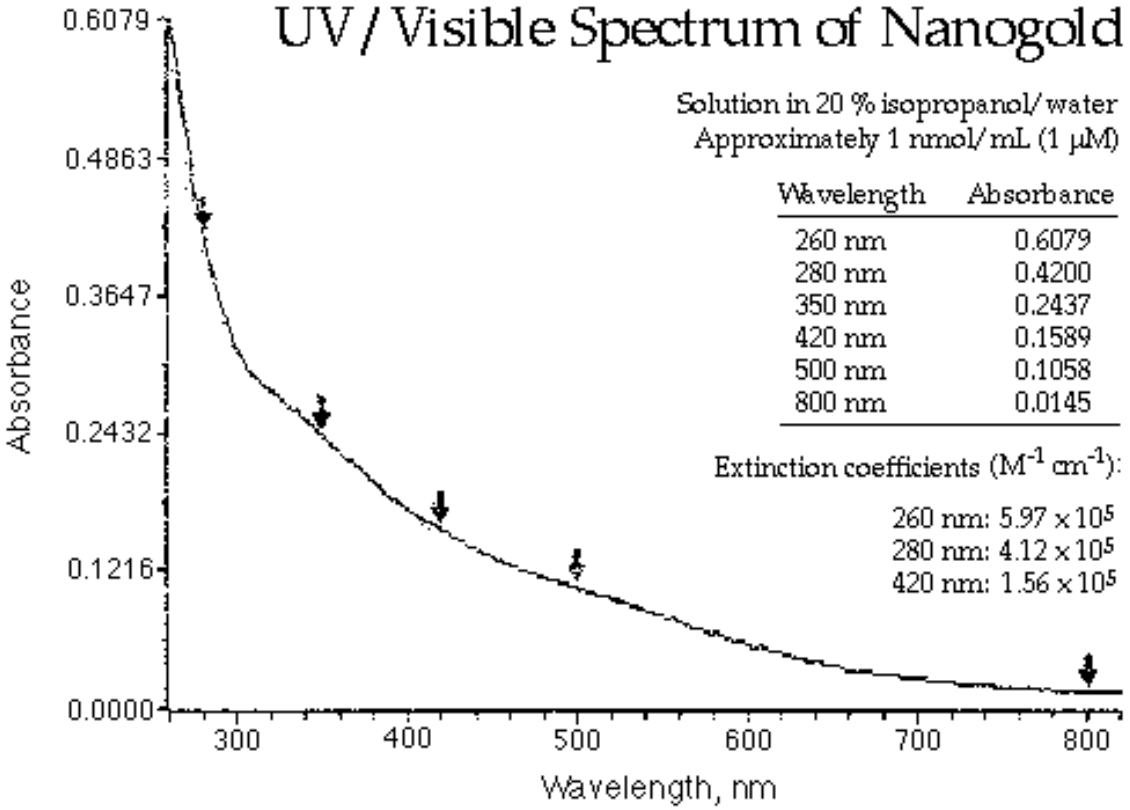

Figure 2. UV/Visible absorption spectrum of Nanogold (Nanoprobes Inc. website).

This would simplify the development of multiplexed assays using QDs with different emission wavelengths. AuNPs have also been shown to provide superior quenching abilities compared with several organic quenchers by Dubertret *et al*. (65). Their work demonstrated higher quenching efficiencies with Nanogold particles over DABCYL (4-([4-(dimethylamino)phenyl]azo benzoic acid) for four different organic dyes.

2.4 Energy transfer mechanisms between quantum dots and gold nanoparticles

2.4.1 Fluorescence Resonant Energy Transfer (FRET)

FRET is an energy transfer phenomenon that occurs when an excited donor molecule is in close enough proximity to an acceptor molecule or quencher (66). Quantum dots can serve as a donor in this process. Organic dyes, quenchers, and metal nanoparticles are all possible acceptors. FRET is modeled as a dipole-dipole interaction and has an energy transfer rate with a $1/R^6$ dependence, where R is the center-to-center distance between donor and acceptor, also termed the Förster radius (67).

2.4.2 Nanometal Surface Energy Transfer (NSET)

NSET is similar to FRET in that they are both considered non-radiative distance dependent energy transfer processes. The Strouse group has referred to this energy transfer process as Nanometal Surface Energy Transfer (NSET) when a AuNP functions as the quencher (68). In this case, the donor-acceptor pair is approximated with a point dipole and an infinite surface (68, 69). This gives the energy transfer rate

$$E_{(NSET)} = \frac{N}{N + (R/R_{0(NSET)})^4} \quad (1)$$

where N is the number of gold nanoparticles and $R_{0(NSET)}$ is the separation distance where quantum efficiency is 50% for N=1. The energy transfer rate or quenching efficiency for FRET has a $1/R^6$ distance dependence. Therefore, the working range for NSET (22 nm) is more than double that of FRET (10 nm) (69).

Mattoussi *et al*. investigated the quenching of QDs by gold nanoparticles by comparing models for FRET, NSET, and dipole-to-metal particle energy transfer (DMPET). The NSET model fit the data better at larger distances when compared to FRET (70).

3 ION DETECTION USING APTAMER-BASED NANOSENSORS

3.1 Design and Synthesis of Aptamer-based Sensors for Ion Detection

3.1.1 Mercury (II) Ion Nanosensor Design with Thrombin Binding Aptamer

In addition to thrombin, the thrombin binding aptamer (TBA) has been used to detect mercury and lead ions with organic dyes and quenchers previously (71). The selectivity of the TBA for Hg and Pb has been previously demonstrated by Liu *et al*. by testing against many other metal ions, including Li, Na, K, Mg, Ca, Cu, Ni, Zn, Cd, Cr, Al, Fe, and Au (71). This research focuses on demonstrating that sensors based on this aptamer are viable when previously tested fluorescent dyes are replaced with QDs, which have superior luminescence, photostability, and lifetimes. To protect the region of the aptamer that is known to be active from any interference from the QD, a 12-Carbon spacer has been used to separate the QD from the aptamer. For these reasons the previously reported selectivity tests were accepted in this study. The previous study showed some affinity for Ni and Fe, but after Pb the largest affinity was for Hg.

The folded structure caused by Hg is different from that of Pb, but it still results in quenching via FRET. However, it was demonstrated that NaCN and random DNA could be used as masking agents to greatly improve the selectivity of TBA for Pb (71). The NaCN interacts with Hg, preventing it from interfering with the Pb detection. To improve selectivity for Hg, phytic acid could be employed as a masking agent. Therefore, the thrombin binding aptamer functions as a very selective molecular recognition element for detecting Hg^{2+} and Pb^{2+} ions.

Oligonucleotides can be used for Hg^{2+} ion detection because they interact with thymine (T) bases to create T-Hg^{2+}-T structures (74). The TBA sequence is 5'-GGT TGG TGT GGT TGG-3'. The symmetry of thymines in the TBA sequence results in a folded hairpin structure when Hg^{2+} is present. This conformational change brings the QD within close enough proximity to the AuNP for the luminescence to be quenched via NSET (Figure 3).

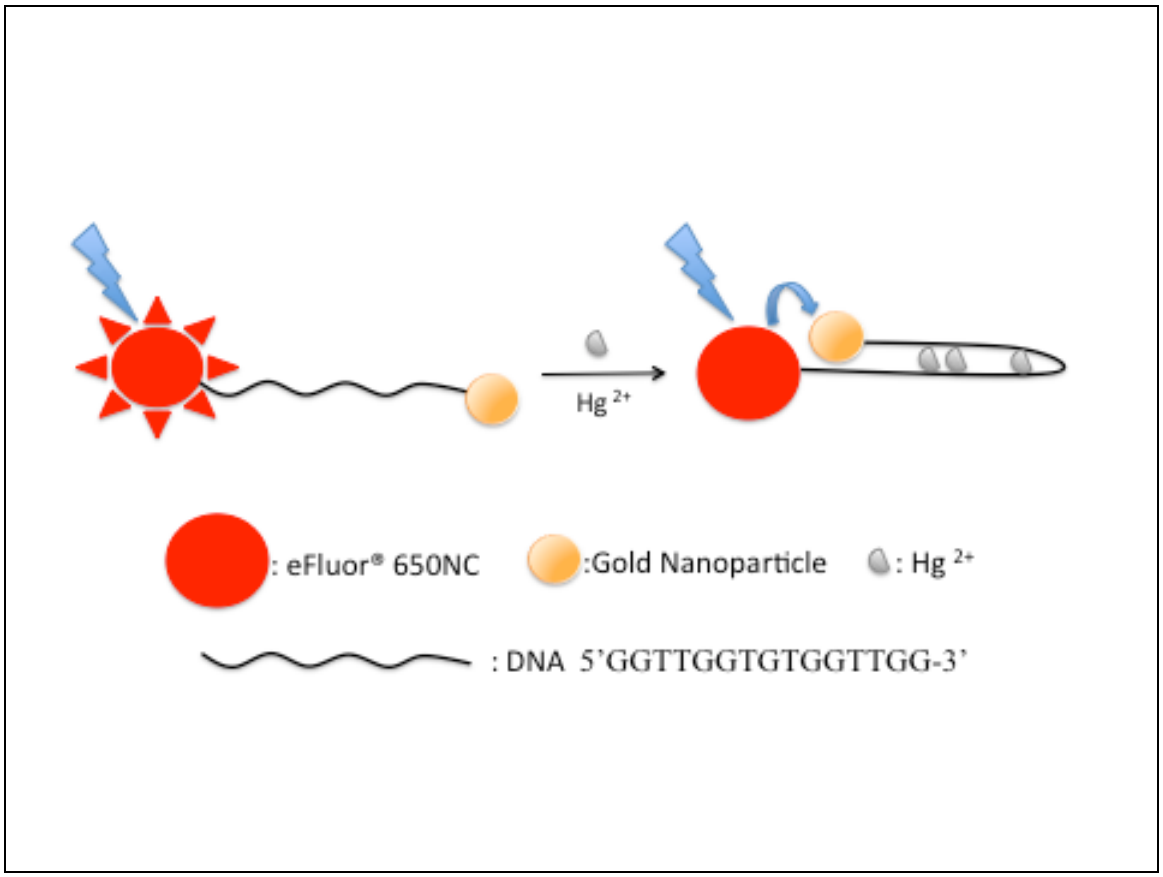

Figure 3. Schematic of the NSET based sensing mechanism of the AuNP-TBA-QD bioconjugate probe for detecting Hg^{2+} ions.

Figure 4 shows how Hg ions interact with DNA through the nitrogen 3 atom of the nucleic acid thymine. This interaction is why a strand of DNA with 6 thymines in it will bind to Hg. Since the thymines are symmetric in their position, the TBA folds in half when the thymine-Hg-thymine structures form.

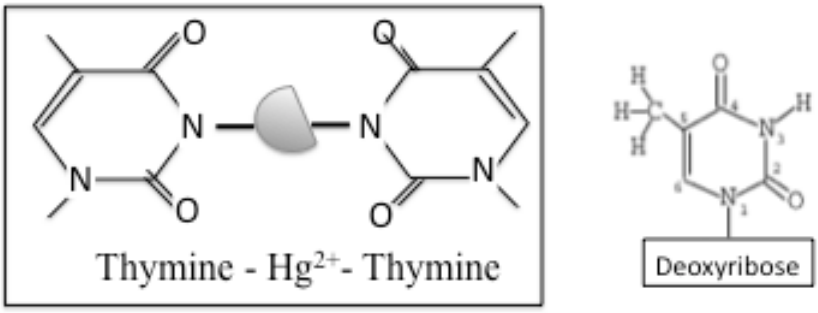

Figure 4. Mercury (II) ions interact with the nitrogen 3 atoms (N3) in the DNA base thymine.

3.1.2 Lead (II) Ion Nanosensor Design with Thrombin Binding Aptamer

Another important feature of the TBA is the position of several deoxyguanosine (G) units, which interact specifically with Pb^{2+} ions to form a G-quartet. The quenching is a result of the G-quartet structure shown in Figure 5, which consists of two square planar arrays of four Hoogsteen hydrogen-bonded guanines. Since the G-quartet structure is stabilized by the Pb^{2+} ion, this conformational change maintains the close proximity of the QD and AuNP

compared to the free coil state of the TBA. The light from the excited QD is transferred via a nonradiative process to the AuNP without emitting any photons. This results in a decrease in photoluminescence or quenching.

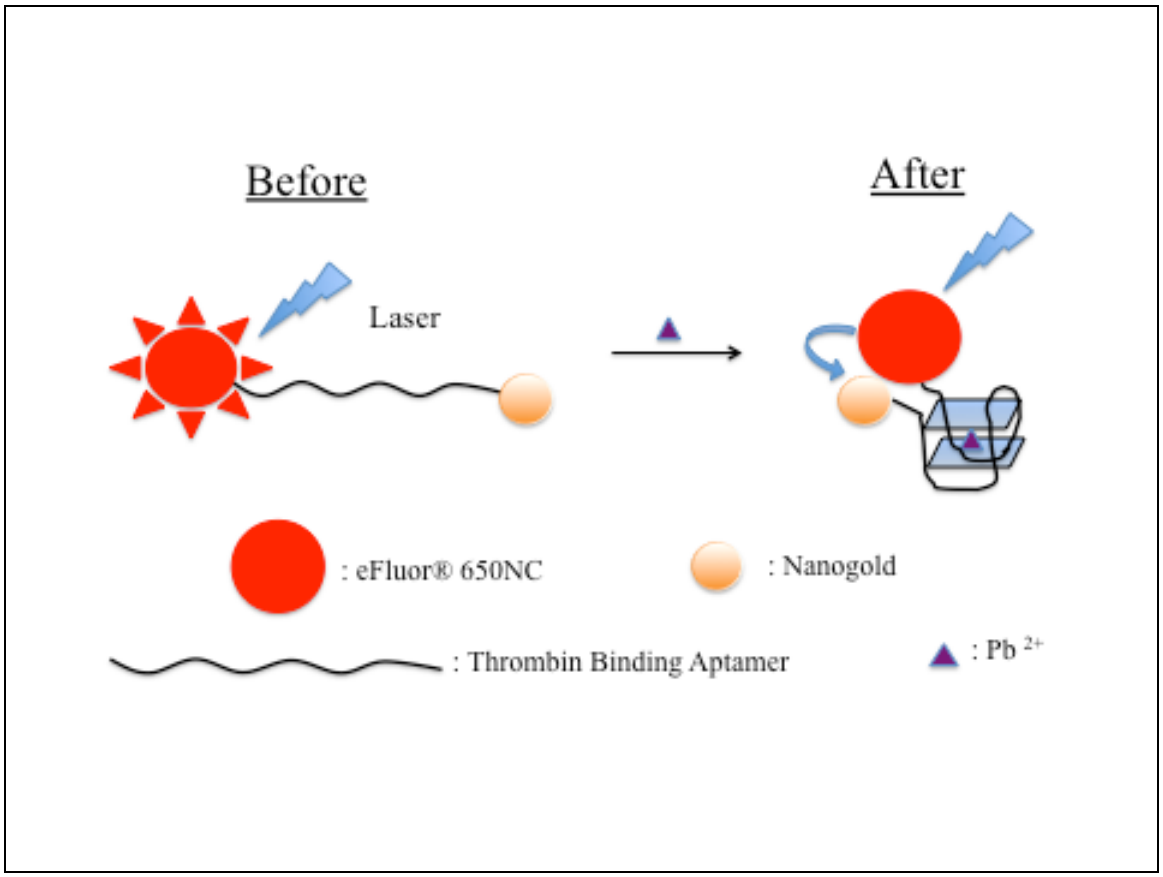

Figure 5. Schematic of the NSET based sensing mechanism of the AuNP-TBA-QD bioconjugate probe for detecting Pb^{2+} ions. The Pb ion causes the G-quadruplex formation seen on the right.

Recently Fu *et al*. have demonstrated Pb^{2+} ion detection using the thrombin binding aptamer as the molecular recognition element and resonant Rayleigh scattering for signal transduction. While this method has the benefit of being label free, it still requires the use of a laser for excitation. Quantum dots can be excited with a simple and inexpensive LED, which makes them more suitable for field use (72). Oligonucleotides known as DNAzymes have been used with QDs to detect Pb^{2+} ions. Wu *et al*. developed a sensor using a Pb DNAzyme, QDs, and organic quenchers. The use of a DNAzyme adds an additional step for hybridizing the two single stranded oligonucleotides (73). Wu *et al*. also used two different organic quenchers for a multiplexed sensor. In the current study, gold nanoparticles are used as quenchers. The advantage here is that AuNPs can absorb light across the visible spectrum and be used for multiple emission wavelengths.

3.1.3 Procedure for Synthesizing Nanosensor for Hg and Pb Detection

The probe is synthesized by two conjugation reactions. The AuNP contains a maleimide group, which allows conjugation to the dithiol functionalized TBA terminus. Carboxyl-functionalized CdSe/ZnS QDs are

bound to the AuNP-TBA conjugates through the amine group on the opposite TBA terminus. The TBA (5'-/AmMC12/GGT TGG TGT GGT TGG/3ThioMC3-D/-3') was obtained from Integrated DNA Technologies Inc. (Coralville, IA). The carboxyl-functionalized eFluor® 650 Nanocrystals (NC) or QDs were acquired from eBioscience, Inc. (San Diego, CA). The carboxyl-functionalized eFluor® 650 Nanocrystals (NC) or QDs were purchased from eBioscience, Inc. (San Diego, CA). They are composed of a CdSe core and a ZnS shell with a hydrophilic coating. The emission wavelength is 650 +/- 3 nm, which is a direct result of the nanocrystal size, which is 8.7 nm in diameter. The diameter of the QD with its coating is 20-26 nm. The monomaleimido Nanogold® particles of 1.4 nm diameter were obtained from Nanoprobes, Inc. (Yaphank, NY). The reagents TCEP (Tris(2carboxyethyl)phosphine) and EDC were purchased from Pierce Biotechnology (Rockford, IL). Nanosep® centrifugal devices in 3K and 100K molecular weight cutoffs (MWCO) were acquired from Pall Life Sciences (Ann Arbor, MI). Lead (II) chloride salt and Mercury (II) Nitrate were obtained from Sigma Aldrich (St. Louis, MO).

The TBA was dissolved in Tris ethylenediamine tetraethyl acetate (EDTA) (TE) buffer (10 mM Tris, 1 mM EDTA) at pH 7.4. EDTA aids in protecting DNA from degradation by nucleases via chelation of divalent cations, which are required for nucleases to function. The dithiol group on the TBA was first reduced using TCEP and then mixed with activated Nanogold solution. Gold nanoparticles and DNA were incubated at a ratio of 7:1 overnight at 4°C. Excess gold was used to ensure that each TBA was conjugated to a AuNP. This was done to aid in preventing false negatives, where QD photoluminescence (PL) does not become quenched, despite the presence of Hg^{2+} or Pb^{2+} ions. An illustration of this is shown in Figure 11.

Next, the solution was filtered using a 3K MWCO centrifugal device at 14,000 x g for 15 minutes, to remove the excess TCEP. The TBA-AuNP conjugates were then resuspended in Borate buffer. Borate buffer is suitable for use in the QD conjugation step, as it contains no amines, which could bind to the functionalized QDs.

3.1.4 Procedure for Gold Nanoparticle and DNA Conjugation

The following procedure was adapted from the Nanoprobes Inc. protocol for binding the Nanogold to a target. The ratio of gold nanoparticles to target molecule is dependent upon the molecular weight (MW) of the target. The procedure below was used for synthesis of the mercury and lead ion sensor using the modified thrombin binding aptamer (TBA), which has a MW of 5233.7 Da. This small MW would indicate an excess of DNA be used, but it was determined that an excess of AuNPs would ensure that all DNA are conjugated (see Figure 11).

1) Dilute stock DNA to a working concentration of 10 μM using TE buffer, pH 7.4.
2) Reduce the disulfide bond on the DNA using TCEP by adding the following to an eppendorf tube:
    a. 86 μl DNA
    b. 7 μl of 0.2 M EDTA
    c. 6 μl TCEP
3) Let sit for 5 – 10 minutes to allow bonds to break
4) Dissolve Nanogold in 20 μl isopropanol and 180 μl Milli-Q water.

5) Once dissolved add to the reduced DNA solution and incubate at 4°C for 24 hours or 2 hours at room temperature.
6) Filter solution for 15 minutes at 14,000 x g using a 3K MWCO centrifugal device to remove the salts (unbound AuNPs will be removed at a later step).
7) Wash twice with Low Sodium PBS Buffer (pH 7.4).
8) Resuspend retentate in Borate buffer (50 mM, pH 7.2).

3.1.5 Procedure for binding DNA-AuNP Nanoconstructs to QD

Two ratios of TBA-AuNP structures to QDs were tested for the TBA to QD conjugation, 10:1 and 5:1. The carboxyl groups on the QDs are activated with the cross-linker, EDC. Once activated, they are mixed with the amine-functionalized end of the TBA and allowed to react for two hours at room temperature while gently mixing. This is done in a glass vial. The solution was then filtered with a 100K MWCO centrifugal device at 5,000 x g for 10 minutes to remove any unbound TBA-AuNP complexes (33). This was followed by a washing step. The washed conjugate was then suspended in TE buffer for testing or storage at a concentration of 1μM.

The ratio of DNA-AuNP conjugate to QD is an important parameter in this conjugation step because it determines the average number of nanoconstructs that are bound to each QD. There is not a uniform number due to the many carboxyl groups on the surface of the QD. Therefore the number of aptamers per QD follows the Poisson distribution. The closer to a 1:1 ratio that can be obtained while minimizing the number of QDs with zero conjugates attached is optimal. For this reason the 5:1 ratio was also tested.

3.1.6 Zinc and Cadmium Ion Detection with Zinc Aptamer

The aptamer Zn-6m2, which was selected for zinc by Rajendran and Ellington, also has an affinity for cadmium ions (34). They found the kinetics to be different for the two ions however, with the reaction being faster for zinc. A truncated version of this aptamer was evaluated as the molecular recognition element in an optical probe for the detection Zn and Cd ions. The truncated form of the Zn-6m2 aptamer was only 50 bases in length, but contained the nucleotides involved in the folding and binding to zinc ions, was purchased from Integrated DNA Technologies Inc. (Coralville, IA). Mfold was used to show the predicted folded structure of the truncated aptamer, which is the structure with

the lowest free energy as shown in Figure 6 (58). It was functionalized on the 5' terminus with a disulfide group and the 3' end contained an amine modification.

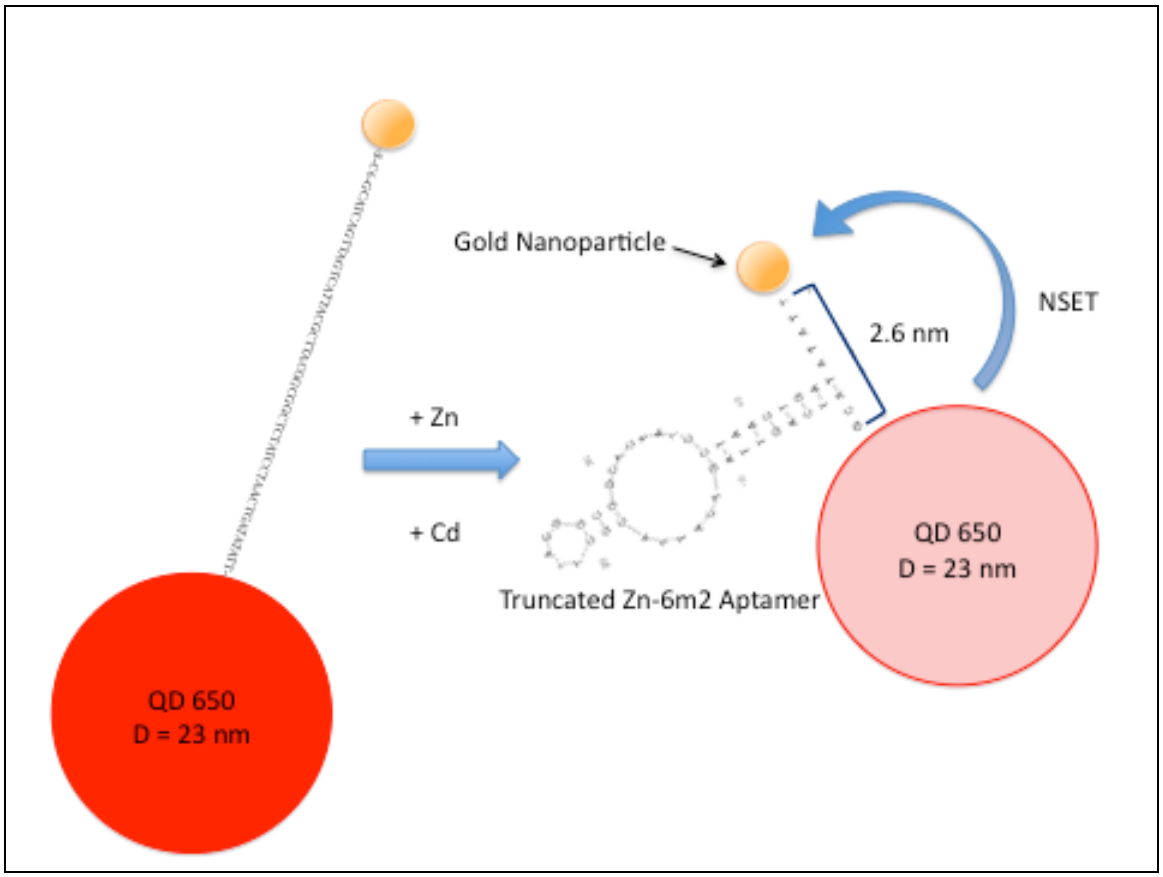

Figure 6. Schematic of the optical detection technique used for the AuNP-Zn aptamer-QD probe for Zn and Cd ion detection. Folded aptamer structure was predicted by mfold.

The carboxyl-functionalized eFluor® 650 Nanocrystals (NC) or QDs were acquired from eBioscience, Inc. (San Diego, CA). These QDs have a CdSe core and a ZnS shell with a polymer coating and an emission wavelength

of 650 +/- 3 nm. The Monomaleimido Nanogold® particles of 1.4 nm diameter were obtained from Nanoprobes, Inc. (Yaphank, NY). The reagents TCEP and EDC were purchased from Pierce Biotechnology (Rockford, IL). Nanosep® centrifugal devices in 3K and 100K molecular weight cutoffs (MWCO) were acquired from Pall Life Sciences (Ann Arbor, MI). Zinc chloride solution (0.1 M) and cadmium nitrate solution were obtained from Sigma-Aldrich (St. Louis, MO).

For the DNA-AuNP conjugation a ratio of 7:1 gold to DNA was used and the reaction was incubated at room temperature for 2.5 hours. The mixture was filtered using the 3K MWCO centrifugal device at 14,000 x g for 15 minutes, then resuspended in borate buffer. Borate buffer is used because it does not contain amine groups, which could interfere with the QD conjugation. The DNA-AuNP nanoconstruct was then conjugated to the QDs at a ratio of 10:1 DNA-AuNP to QD. After activating the carboxyl groups on the QD surface using EDC, the DNA-AuNP was added and the mixture incubated for 2 hours while gently mixing. The reaction mixture was then filtered using a 100K MWCO centrifugal filtration device at 5,000 x g for 15 minutes to remove any unbound

DNA or AuNPs. The filtration step was repeated twice using borate buffer to further wash away any unbound materials.

3.2 Photoluminescence Measurement Results for Liquid Assays

The PL measurements were taken with a USB4000 Ocean Optics (Dundelin, FL) spectrometer with the SpectraSuite software. The light source was a 380-nm LED, also purchased from Ocean Optics. Both components are small enough to be portable and the spectrometer can easily be integrated with a tablet computer or smart phone for field use. A diagram of the set up used is illustrated in Figure 8. The liquid assay was placed in a UV cuvette for PL measurement. In order to decrease the amount of excitation light received by the detector, the source and detector fiber optic cables were oriented at right angles. A filter was also used to reduce the UV frequencies. Finally, the software was used to subtract the background from the spectra.

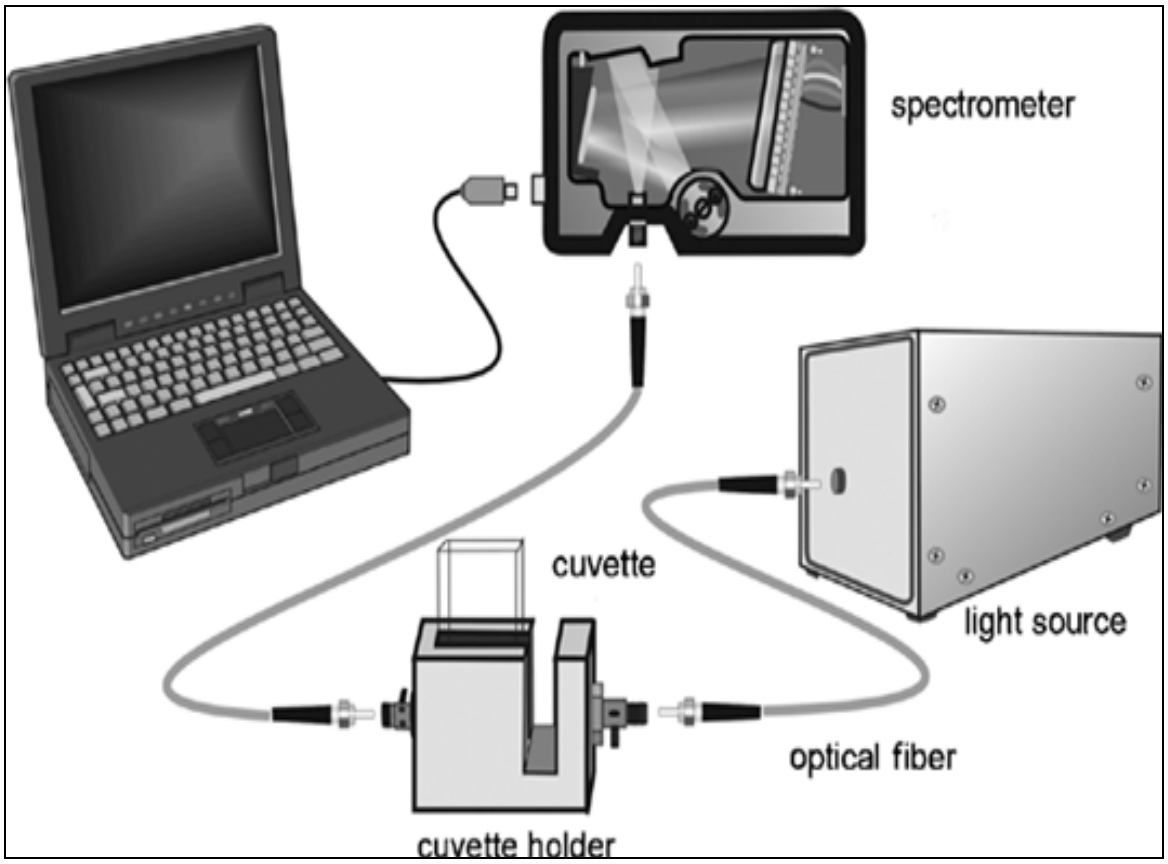

Figure 8. Diagram of the Ocean Optics spectrometer set up for PL measurements using cuvette for liquid samples.

3.2.1 Liquid Assay PL Results – Hg Detection

Three aliquots of TBA probe (10 nM) were prepared for analysis, one without Hg^{2+}, one containing 500 nM Hg^{2+} ions, and the third containing a large excess of 824 μM Hg^{2+} ions. The sample volume used was 100 μL.

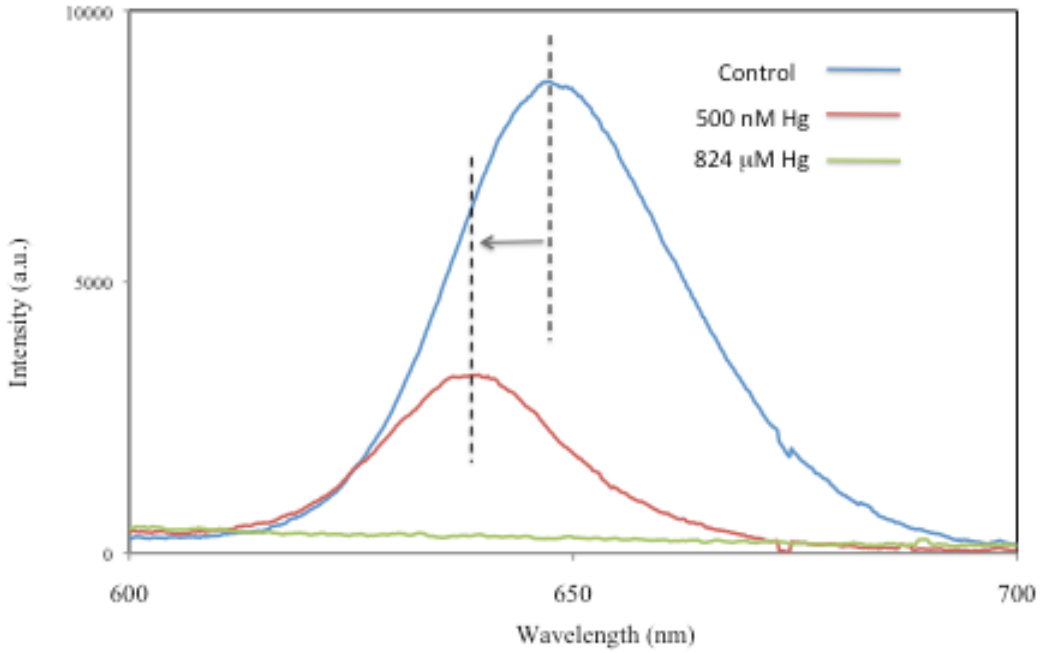

Figure 8. Fluorescence spectra of AuNP-TBA-QD nanoconstruct (10 nM) control (blue), 500 nM Hg^{2+} (red) and 824 μM Hg^{2+} (green). There is a blue shift between the control and the 500 nM Hg spectra.

Figure 8 shows the photoluminescence spectra of the three samples, where a decrease in photoluminescence peak is seen with Hg^{2+} ions present. The quenching efficiency was calculated as $[(I_0 - I_{Hg})/I_0]$, where I_0 is the peak luminescence intensity without Hg^{2+} for 10 nM TBA probe and I_{Hg} is the peak luminescence intensity with Hg^{2+} ions present. The 500 nM Hg^{2+} ion sample

had a quenching efficiency of 62%. This was comparable with the work of Liu *et al*. who obtained 66% quenching efficiency using the TBA with the donor carboxyfluorescein (FAM) and the acceptor DABCYL for Hg^{2+} sensing at 500 nM (71).

In addition to the luminescence quenching seen with Hg^{2+} present, there was also a blue shift between the unquenched and quenched samples. The peak for '0 Hg' in Figure 8 is at 648 nm, whereas the peak for the quenched state with 500 nM Hg, is shifted 13 nm to 635 nm. This decrease in emission peak has been demonstrated previously in our group through an investigation of the energy transfer process between QDs and AuNPs, where a 12 nm blue shift was seen (18). In both cases, 1.4 nm diameter Nanogold particles and CdSe/ZnS QDs were used.

3.2.2 Effect of Hg on QD PL

When the nanosensor was tested against a large excess of Hg^{2+} ions, 824 μM, there was no peak detected. It is unlikely that complete quenching would be achieved by the probe mechanism because statistically there are a

small number of unconjugated QD present in the assay. Using a ratio of TBA:QDs of 10:1 gives a distribution of QDs with different quantities of TBA attached and there would be less than 0.01% of QDs with no TBA bound. The Hg2+ ions would not be able to cause quenching through the expected mechanism for those unconjugated QDs. There would still be some fluorescence emission from the unbound QDs. There would have to be another means of extinguishing the fluorescence. Alternatively, the complete quenching observed could be the result of the Hg2+ ions interacting with the surface of the QDs and thereby affecting their emission. A quenching effect was seen in other work using L-cysteine capped CdS QDs when exposed to Hg2+ ions (16). Moreover, the heavy metals Cu^{2+}, Fe^{3+}, and Zn^{2+} have been shown to eliminate QD fluorescence irreversibly (78). Therefore, it is possible that the extinguished photoluminescence could be the result of mercury ions interacting with the QDs.

This was tested by exposing unconjugated QDs to mercury (Figure 9). The photoluminescence was measured for a solution of 10 nM QDs (no TBA-AuNP nanoconstruct attached) as control. Next the QD solution was exposed to

the same Hg2+ ion concentrations tested against the sensor. As shown in Figure 9 below, the peak intensity for the QDs alone and the QDs with 500 nM Hg2+ ions is effectively the same. Interestingly, the addition of 824 μM Hg2+ resulted in the complete quenching of the QD luminescence. At a certain concentration, Hg^{2+} ions also eliminate QD fluorescence, but below this level the aptamer-based probe is necessary for detection.

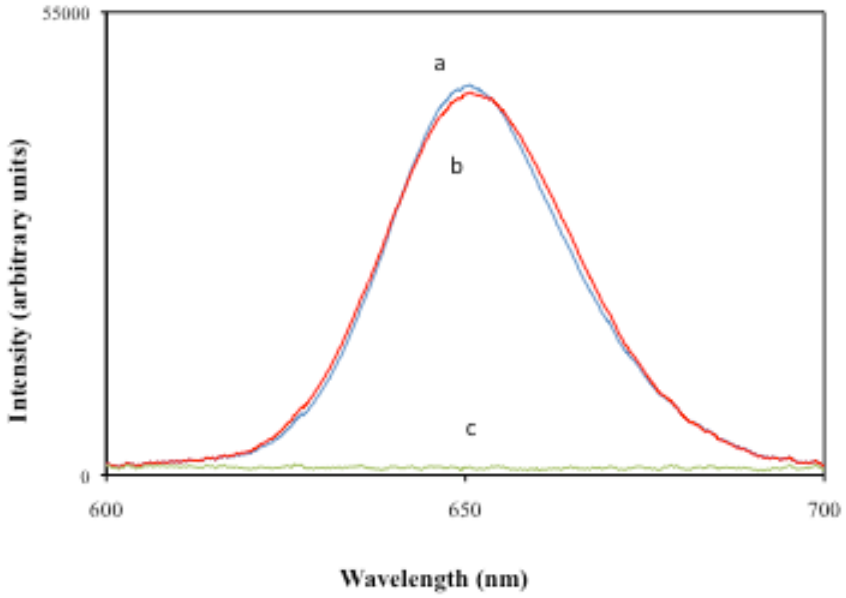

Figure 9: Fluorescence spectra of (a) QDs (10 nM), (b) QDs with Hg^{2+} (500 nM), and (c) QDs with Hg^{2+} (824 μM) present.

A range of Hg concentrations were tested against unconjugated QDs to find what level eliminated fluorescence completely and at what concentration do Hg^{2+} ions begin to interfere with QD PL. For a 10 nM sample of QDs complete inhibition of fluorescence occurs between 45 and 55 μM mercury (II) ions (Figure 10).

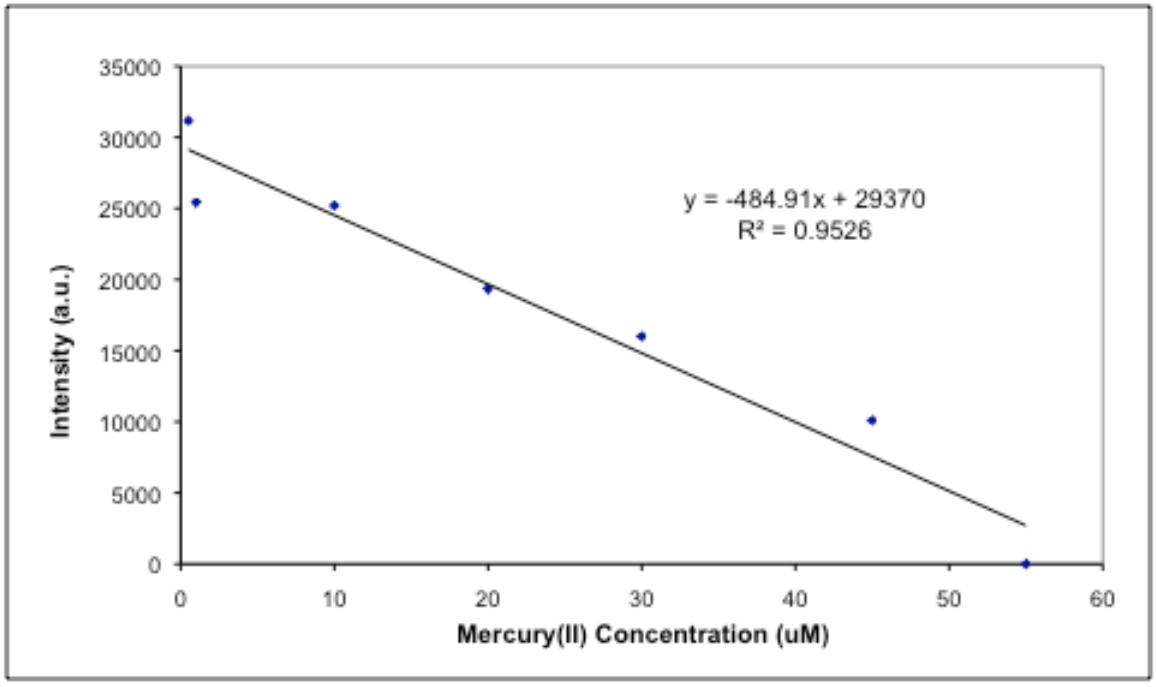

Figure 10. Photoluminescence (PL) peak intensity of 10 nM QD650 versus Hg ion concentration from 0.5 μM to 55 μM.

The PL intensity at 1 μM and 10 μM Hg are not significantly different and the peak intensity at 0.5 μM actually increases. However, at 20 μM Hg there is a significant change in PL of -29%.

3.2.3 Synthesis Optimization for Gold Nanoparticle Conjugation

While detection of mercury ions has been demonstrated, there has been variability in the probe performance. It was hypothesized that using an excess of DNA in the conjugation of the gold nanoparticles to the DNA may improve performance. This was based on the actual probe configuration as shown in Figure 11 where each QD has approximately 10 DNA strands attached. The ideal configuration would be just one DNA sequence per QD. However, the difficulty in separating QDs with different numbers of DNA strands attached prevents this. Given this configuration it is important that each strand of DNA is conjugated to an AuNP. If not, false negatives are more likely, as illustrated in the bottom row of Figure 11, where the QDs are not quenched in the presence of Hg. If Hg ions interact with DNA that does not have a gold nanoparticle attached, then the folding event will not result in quenching.

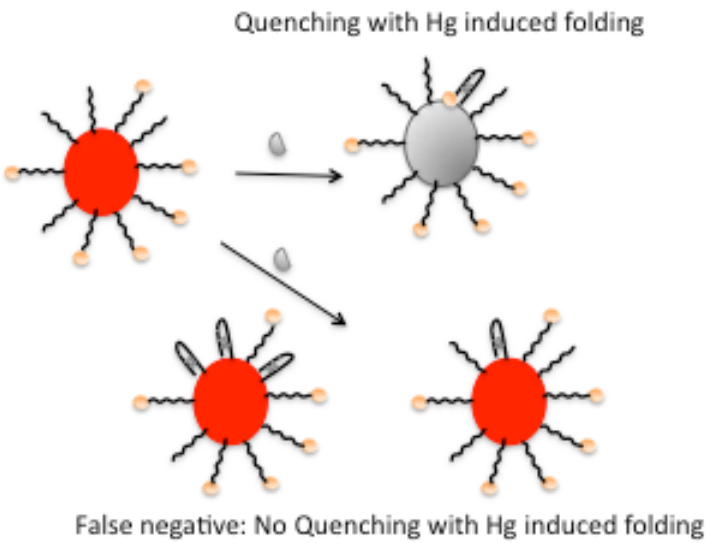

Figure 11. Actual probe configuration when using 10:1 DNA to QD ratio. Illustrates possible scenario if some DNA aptamers do not have a gold nanoparticle attached; a false negative could result.

In order to ensure that all DNA are conjugated to a AuNP, an excess of gold (10-fold) was tested in the gold conjugation step. Since the AuNPs are 1/20th of the diameter of the QDs, they will be removed during the filtration step of the QD conjugation. The excess gold showed better results so different ratios were tested. In addition to the 10:1, 7:1, 5:1, and 3:1 were evaluated. This was done to reduce materials used if possible. A ratio of 7:1 for AuNP:DNA was

found to have the most consistent results and all future probe fabrication was done using this optimized parameter.

The ratio of DNA to QD used in the second conjugation step was also investigated through testing of DNA:QD ratio 5:1 against the control ratio of 10:1. A 5:1 ratio would produce mostly QDs containing 5 DNAs attached to each. The liquid assay probe was tested in triplicate at a range of concentrations for Hg^{2+} and Pb^{2+} ions, between 100 nM to 10 μM for both DNA to QD ratios. The PL intensity at 650 nm was recorded for the probe and the probe plus mercury. The average of three measurements was taken to gauge the uniformity of the probe. Quenching efficiency (η%) was calculated using the formula,

$$\eta = (I - I_0)/I_0 \qquad (2)$$

where I_0 is the intensity of the nanosensor assay and I is the intensity of the assay exposed to target ions. This results in a decrease in photoluminescence or quenching so η is given as a negative percent.

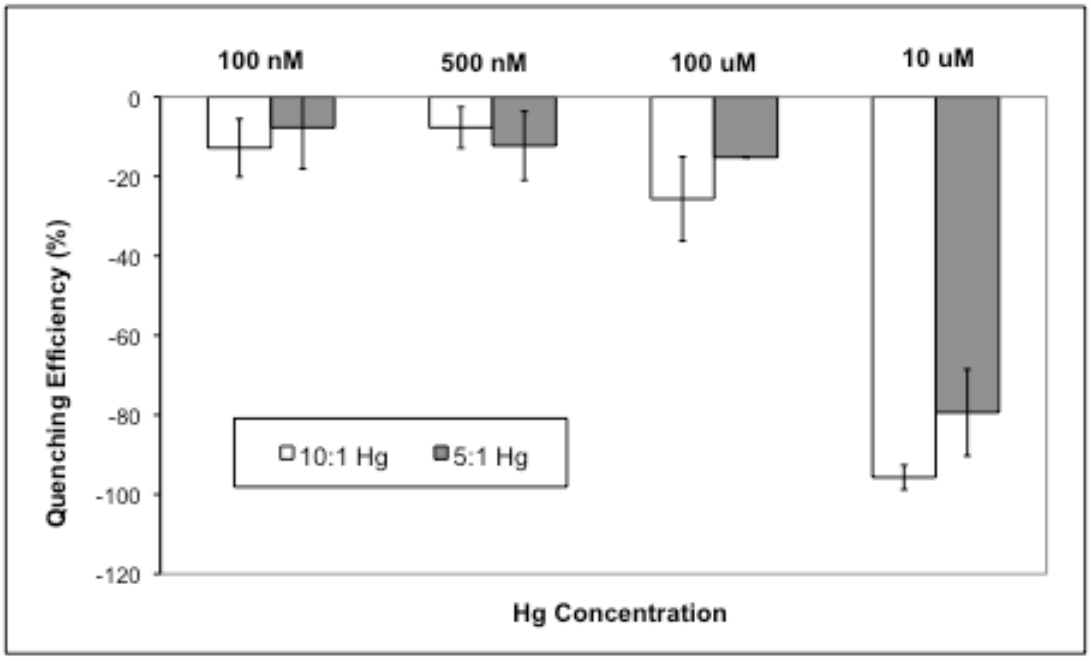

Figure 12. Quenching efficiency vs. Hg concentration for different DNA:QD ratios in liquid assay

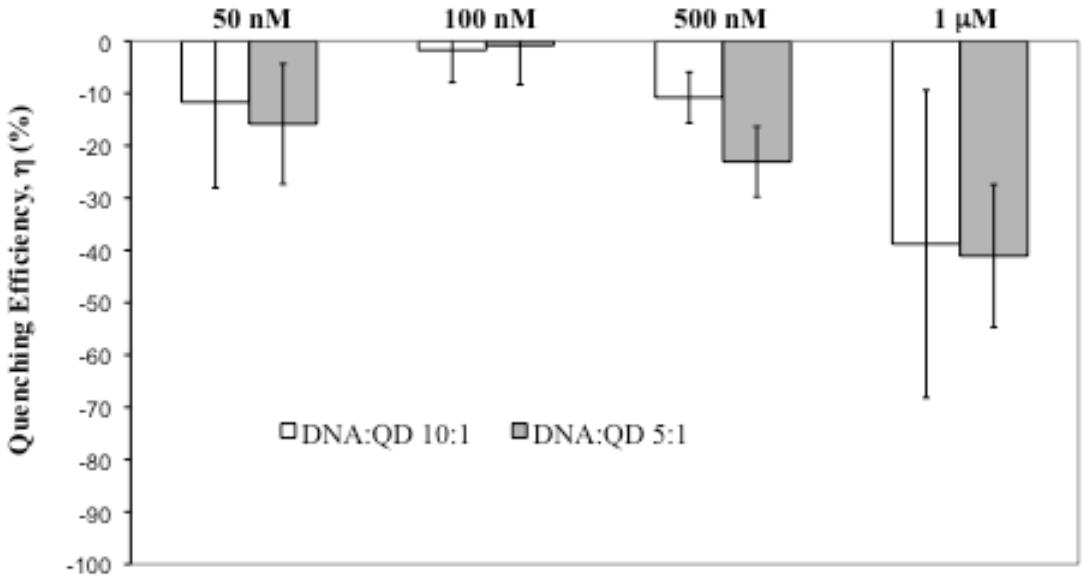

Figure 13. Quenching efficiency of the probe at different Pb concentrations for different DNA to QD ratios tested in a liquid assay

Figure 13 shows the results of the liquid assay probe being tested against different concentrations of lead from 50 nM to 1 µM for 10:1 and 5:1 DNA to QD ratios. Initially, a ratio of 10:1 was used for DNA to QD conjugation reaction. This results in an assay in which the majority of the QDs have 10 TBAs bound to the surface. The 5:1 ratio was tested to determine if it would improve the sensor sensitivity by presenting only five aptamers per QD available for interaction. The more TBA-AuNP conjugates bound to each QD,

the lower I_0 will be, based on equation (1), where the energy transfer rate is proportional to the number of AuNPs. Since only one Pb^{2+} ion is required to change the TBA from a random-coil to a G-quartet, it may perform with greater sensitivity with fewer aptamers per QD. TBA also interacts with K^+ ions to form a G-quartet, but this conformation requires two K^+ ions and forms a less stable structure (77).

The quenching efficiency was calculated for three sets of readings and the average was taken. The error bars represent the standard deviation. The quenching efficiency observed at 1 μM Pb^{2+} ion for the 5:1 and 10:1 ratio assays was -41% and -39% respectively, as shown in Figure 13. The probe was tested at this particular concentration range because the OSHA and the WHO safety levels for lead intake are 30 μg/dl (1.45 μM) and 40 μg/dl (1.93 μM), respectively (37). Blood lead levels above these thresholds are cause for concern. Therefore, a significant quenching efficiency would be required for this range. Based on these results, there is not a significant increase in quenching efficiency for the 5:1 compared to the 10:1 at 1 μM. However, the 10:1 assay has greater variability between readings. Moreover, the 500 nM test did show

greater quenching for the 5:1 sample. The decrease in DNA:QD ratio does appear to improve sensor performance slightly. Reference (71) reports detection levels of 300 pM; however, the sensor developed in this study incorporates QD tags, which have superior anti-bleaching properties and are brighter than fluorescent dyes.

3.2.4 Effect of Pb on QD PL

The QD650 fluorescence was also measured against lead (II) ions to determine if there was interference with the QD luminescence and at what concentration threshold. PL also decreased for Pb, but much less effectively (Figure 14). A nearly 50% reduction was seen at ca. 6 μM, but PL was not completely eliminated at 900 μM.

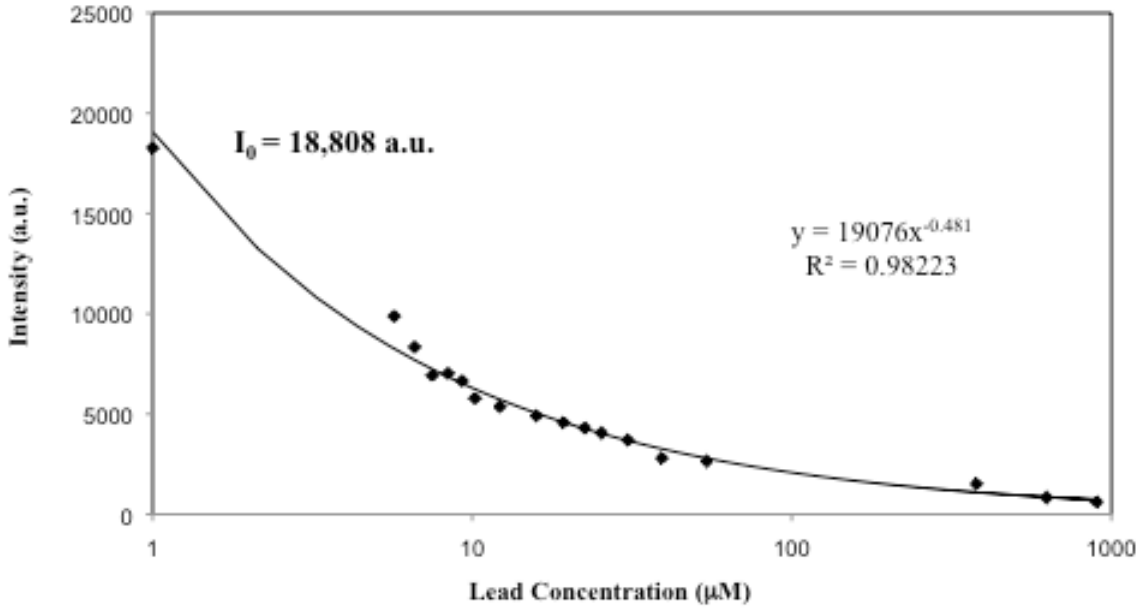

Figure 14. Photoluminescence (PL) peak intensity of 10 nM QD650 versus Pb ion concentration from 0 (I_0=18,808 a.u.) to 900 μM.

QDs exposed to 1 μM Pb^{2+} ions had a quenching efficiency of only -1.3%, compared to approximately -40% for the nanosensor at the same concentrations. The QD photoluminescence was affected at higher lead concentrations, with the quenching efficiency being -47% at just below 6 μM Pb^{2+} ions. This lead level is approximately five times the safety level. This demonstrates that the probe performance for detecting Pb^{2+} ions at 1 μM was

not due to the interaction of Pb^{2+} ions with the QDs. Rather; significant decreases at 1 μM lead are a result of the energy transfer process of the probe.

The extremely high surface area to volume ratio of quantum dots results in large surface state effects. The photoluminescence could be affected by interactions with the surface of the quantum dot (79).

3.2.5 Liquid Assay PL Results – Zn/Cd Detection

Samples were prepared for testing the Zn-6m2 probe against zinc and cadmium. 200 μL samples with a probe concentration of 10 nM were prepared. Each sample was comprised of 2 μL of probe and between 178 μL and 196 μL of Tris-acetate buffer at pH 7.35. After the control intensity was measured, the zinc or cadmium solution was added to make 200 μL. For Zn 100 μM, 800 μM, and 10 mM concentration was evaluated based on the upper limit of normal blood-Zn levels being approximately 20 μM. The calculated quenching efficiencies are shown in Figure 12 below. The integration time was 500 ms. Two measurements were taken for each concentration and averaged.

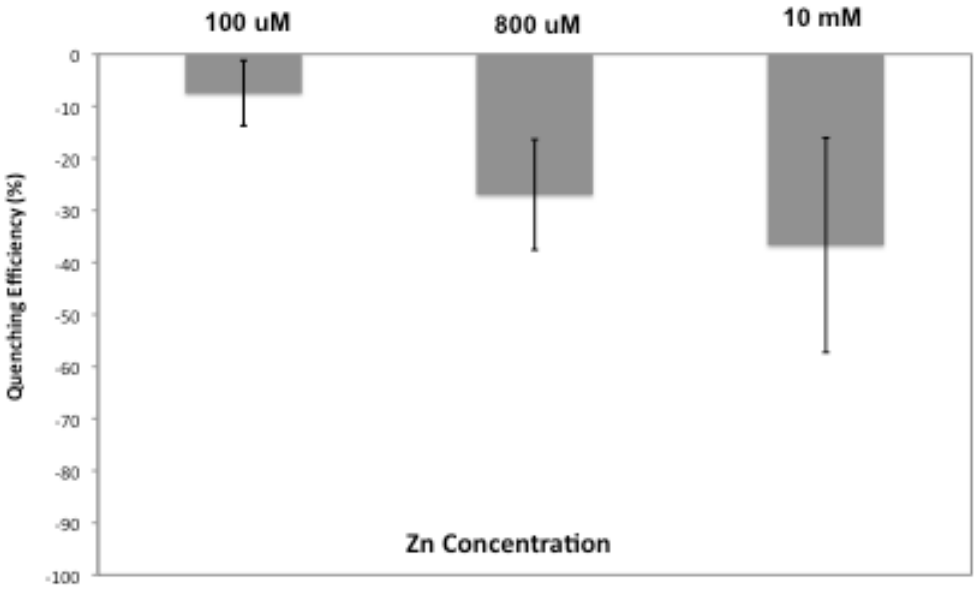

Figure 15. Zn-6m2 aptamer probe tested against different concentrations of zinc (II) ion in a liquid assay. Upper limit for normal blood Zn levels is ~ 20 μM.

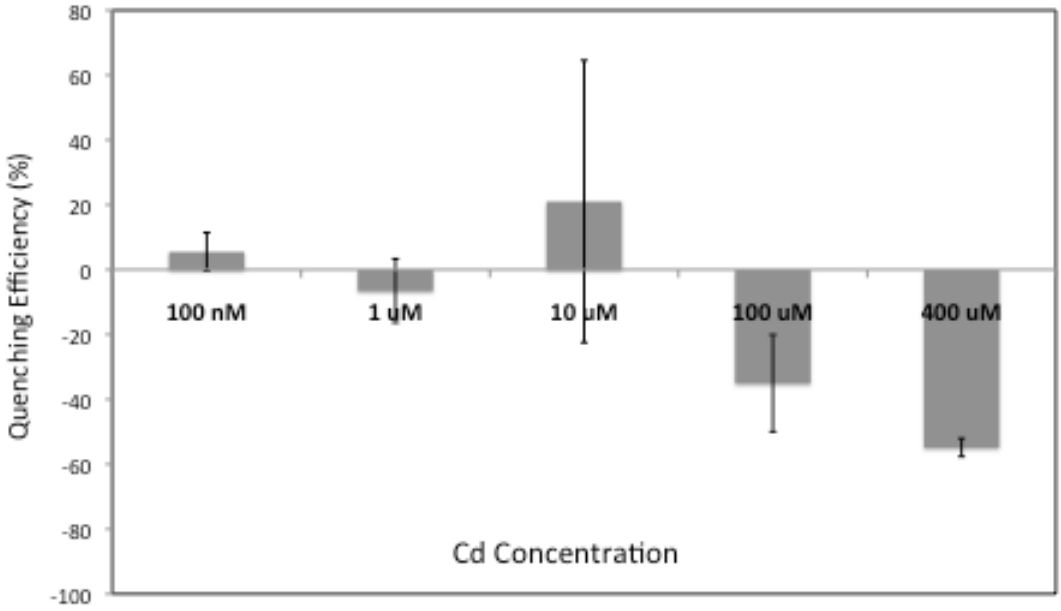

Figure 16. Zn-6m2 probe tested against different concentrations of cadmium (II) ion in a liquid assay.

For cadmium a lower concentration range was tested. These samples also had a final volume of 200 μL and contained 10 nM concentration of probe. The quenching efficiencies are shown in Figure 13 for 100 nM up to 400 μM Cadmium ion concentration. Two measurements were taken and averaged. The Zn-6m2 probe performed well at 100 μM and 400 μM Cd concentrations with significant quenching efficiencies of -35% and -55% respectively.

3.3 Filter Paper Coupon Fabrication

Metal ions are also detected by applying the probe to a filter paper coupon, which could potentially be used in a handheld device. The filter paper used was Immobilon®-FL filter paper from Millipore Corporation (Billerica, MA). The Immobilon®-FL filter paper is meant for use in fluorescence measurements, as it has low auto-fluorescence. The coupon is made by adhering filter paper to a plastic cover slip for rigidity. Two µls of the probe assay are then pipetted onto the filter paper and allowed to dry. Each dot contains 0.6 pmoles of probe. The peak fluorescence intensity of the dot is measured. After the control intensity is recorded a metal ion solution is applied to the dot via pipette and the intensity is measured again. The metal ion target solution concentrations were determined to provide equivalent exposures as the liquid assays. Measurements were taken in duplicate for the filter paper testing.

3.4 Filter Paper Coupon PL Results

The probes synthesized for Hg and Pb and Zn and Cd detection were applied to Immobilon®-FL (low auto-fluorescence) filter paper coupons. Each

dot contained 0.6 pmoles of probe. Once dry, the peak fluorescence intensity of the dot is measured and recorded as the control intensity or I_0. After the control intensity is recorded a volume between 2 µL and 4 µL is applied to the dot via pipette and the intensity is measured again in order to calculate the quenching efficiency. The metal ion solution concentrations were determined to provide equivalent exposures as the liquid assays. Measurements were taken in duplicate for the filter paper testing. For Hg and Pb both DNA:QD ratios were evaluated. In Figure 17 the filter paper coupons made with the TBA probe are tested for a wide range of Hg concentrations. The quenching efficiencies were not significantly different for the 10:1 and 5:1 DNA to QD ratios.

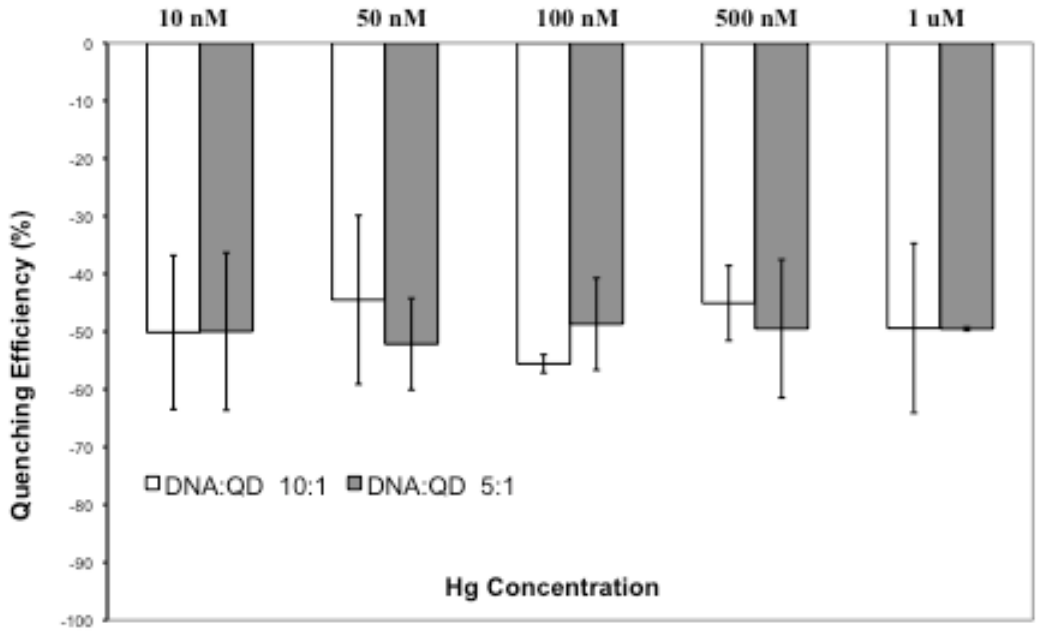

Figure 17. Quenching efficiency of the probe at different Hg concentrations for different DNA to QD ratios tested on filter paper coupon.

When tested against 1 μM Pb^{2+} ion concentration, as shown in Figure 18, the quenching efficiency was -71% for the 5:1 sample and -60% for the 10:1. For both DNA:QD ratios, the standard deviation was below 0.5 for 1 μM Pb^{2+}. Optimal performance at 1 μM is desired for Pb detection based on the WHO and OSHA standards. However, for the 1 μM Pb^{2+} measurement where

the variability between readings was lowest, the 5:1 showed a slightly greater quenching efficiency than the 10:1 for the filter paper coupons.

The filter paper coupon was tested against Cd at three different concentrations (Figure 19). All three concentrations had a quenching efficiency of approximately -60%. The Zn-6m2 probe was also tested against Zn on the filter paper coupons. The quenching efficiencies for 667 nM Zn, 67 μM Zn, and 3 mM Zn are shown in Figure 20.

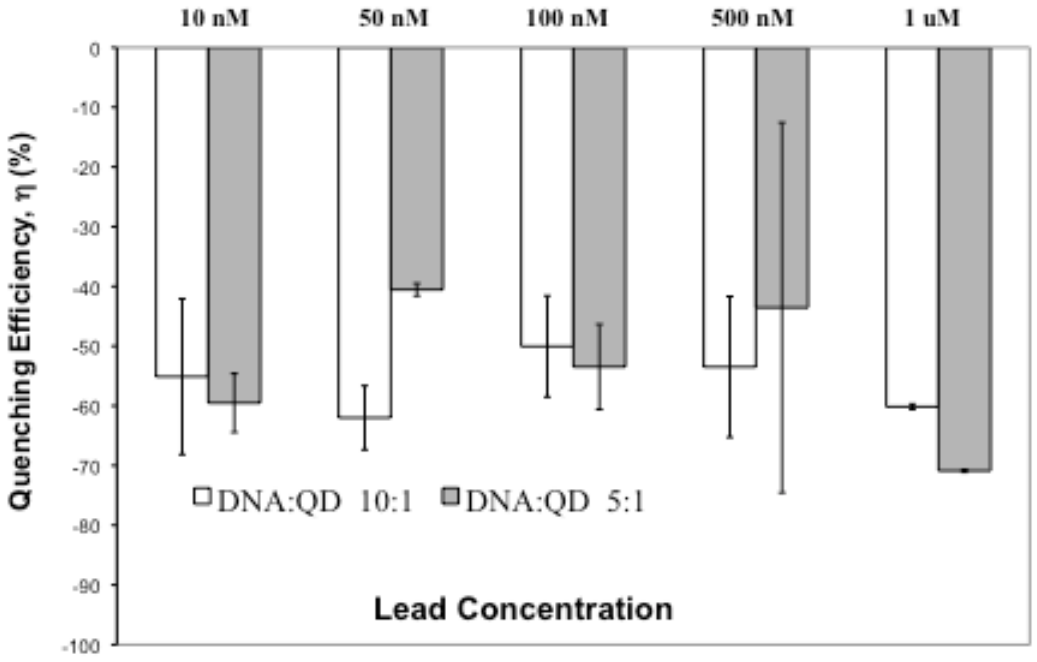

Figure 18. Quenching efficiency at different Pb concentrations on filter paper for different DNA to QD ratios.

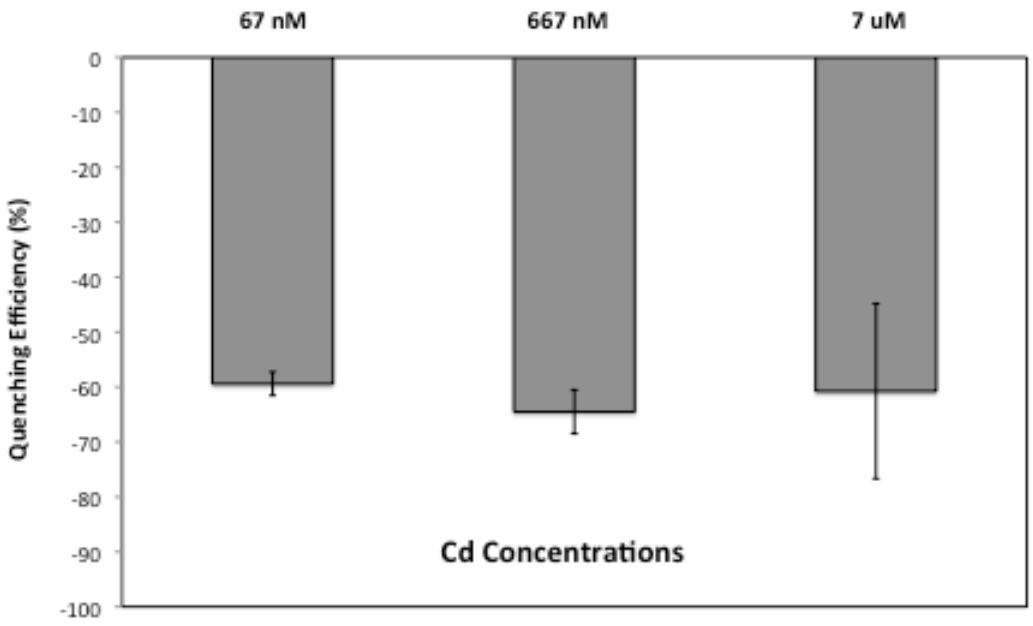

Figure 19. Filter paper coupon tested for three concentrations of Cadmium (II) ion.

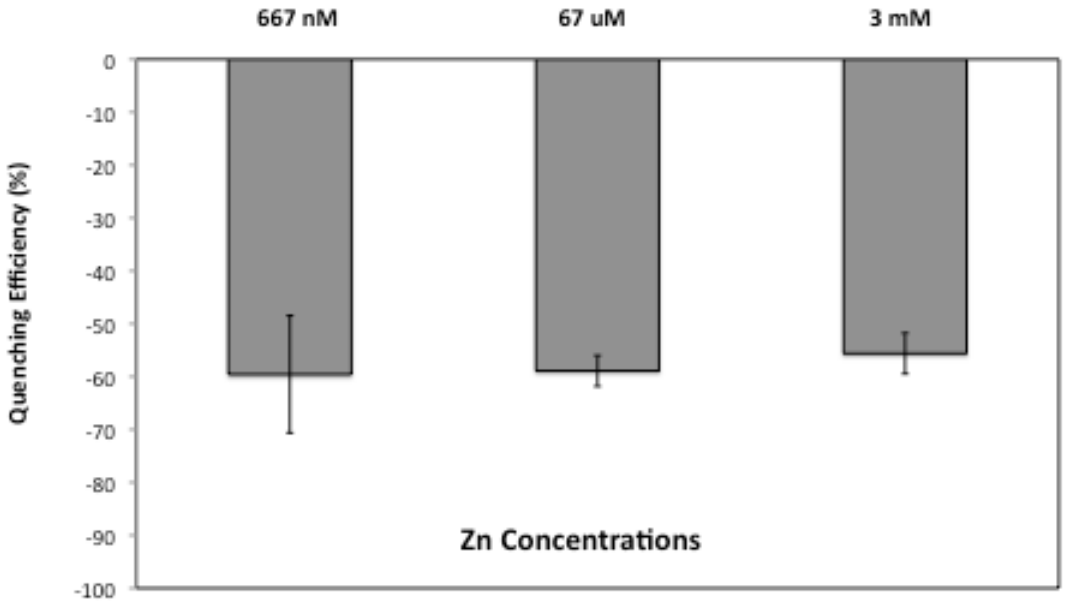

Figure 20. Filter paper coupon tested for three concentrations of Zinc (II) ion.

The liquid assay for Hg/Pb has been shown to be fairly stable after storage at 2-4°C for 3 weeks when tested on filter paper for Hg concentrations between 1.25 μM and 5 μM. The quenching efficiency for 2.5 μM was -56% when tested 1 week after it was synthesized and only decreased to -33% when tested 2 weeks later. The stability of the filter paper coupon dot was also evaluated. In this test the detection of Cd was tested at day 1 for 67 nM concentration with a quenching efficiency -59%. After making the coupons, they

were stored at room temperature for 1 week, and then tested against the same Cd concentration (Figure 21). The quenching efficiency decreased to -45% and had more variability between measurements but still had detection capabilities after being stored at ambient conditions for 1 week.

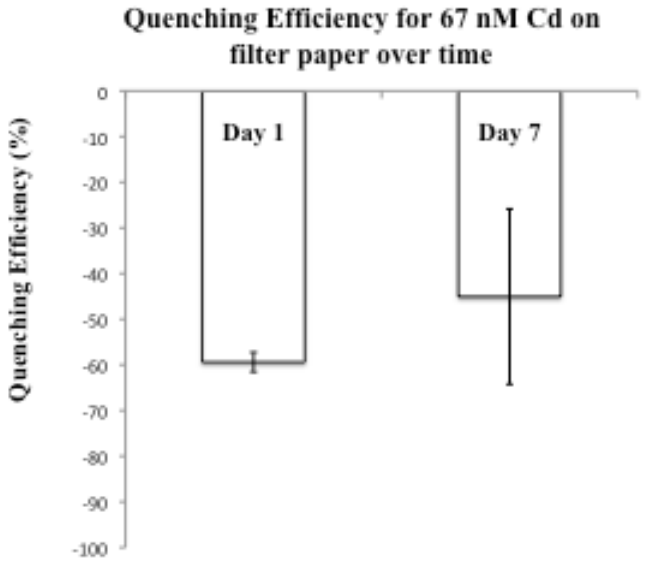

Figure 21. Filter paper coupon assay tested against 67 nM cadmium at two time points to evaluate stability of coupon.

The filter paper coupons were designed for use in a portable hand held device that would contain a detector/filter and light source (LED). The design of this device is shown below. Once the filter paper containing the assay is

exposed to the sample, it would be placed in the device for reading. These filter paper coupons would be disposable or single use sensors.

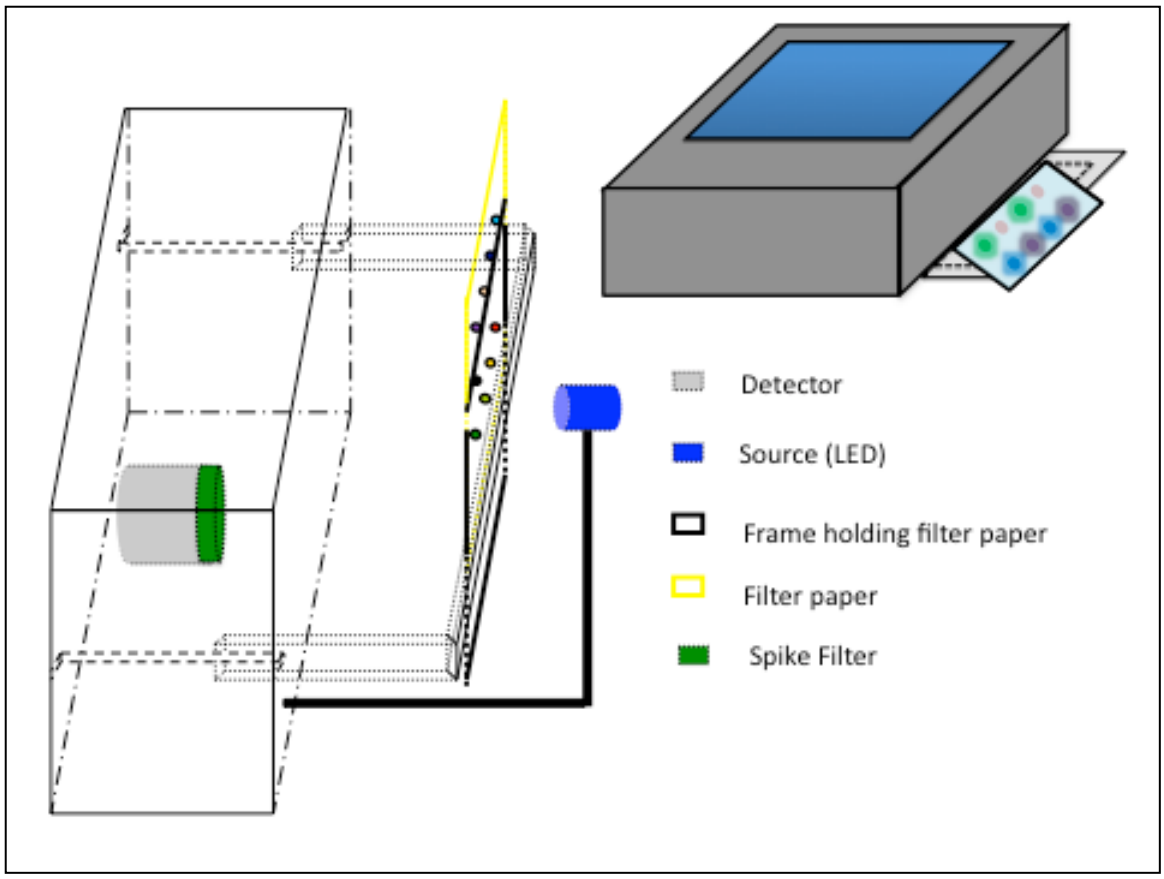

Figure 22. Design of portable hand held device for heavy metal detection. Filter paper frame moves to position each assay between LED and detector/filter for separate readings at same wavelength.

4 THZ SPECTRAL ANALYSIS OF DNA APTAMERS

4.1 Surface-enhanced Raman Spectroscopy (SERS)

Surface-enhanced Raman scattering (SERS) is a phenomenon used to enhance the signal produced by Raman scattering. Raman spectroscopy is a useful tool for sensor development with potential for remote sensing. Raman spectra provide information on the vibrational modes or phonons, between and within molecules. Therefore, you can produce a unique spectral fingerprint for single molecules. SERS is accomplished through the use of substrates with nanometer scale geometries made of metals with many free electrons, such as silver, gold, or copper. Silver is the best choice for frequencies in the visible range and has the lowest damping rate when compared to Au, Cu, and Al (80). These metals produce surface plasmons, which are oscillating electrons, when excited with a laser. The predominant theory on why SERS causes large enhancements of Raman signals is mainly explained by the electromagnetic properties of nanostructures (81). The strong localized surface plasmons produced on the surface of the metal by laser excitation enhance the Raman scattering of the molecule near the metal surface. This enhancement is important because Raman cross sections are between 10^{-31} and 10^{-29}

cm^2/molecule, compared to fluorescence cross sections which are up to 10^{-16} cm^2/molecule. Furthermore, the Raman signal is proportional to the Raman cross-section, the excitation laser intensity, and the number of molecules in the field of detection. Therefore, by enhancing the signal via SERS, fewer molecules are required for a sufficient signal to be produced.

Optical techniques such as Raman scattering and photoluminescence are widely appreciated as potent tools for the study of the optical, electronic, and vibrational (thermal) properties of materials including those relevant to these studies including: semiconductor nanostructures such as quantum dots; biomolecules including DNA, RNA, and aptamers; and nano-complexes based on constructs that incorporate both semiconductor nanostructures and biomolecules. In this study, techniques for advancing the state-of-the-art in the use of these optical tools will be explored to facilitate the step-by-step diagnosis and analysis of the nanoconstructs being fabricated for biomedical applications such as detection of ions and biomolecules using potentially self-administered tests. Of special emphasis in this portion of the research will be an attempt to optimize Raman signature spectra for DNA aptamers using SERS substrates.

Moreover, changes in the SERS signature of DNA aptamers with and without the analyte present are investigated.

4.2 Zinc Aptamer on Silver Film Over Nanosphere SERS Substrate

In order to study the Raman signature of a DNA aptamer that was selected for zinc, a AgFON substrate was used to enhance the signal. The original aptamer, labeled Zn-6m2, that was selected by Rajendran and Ellington was truncated to only include the segment involved in the folded structure (34). The figure below shows the predicted structure of the aptamer when zinc is present.

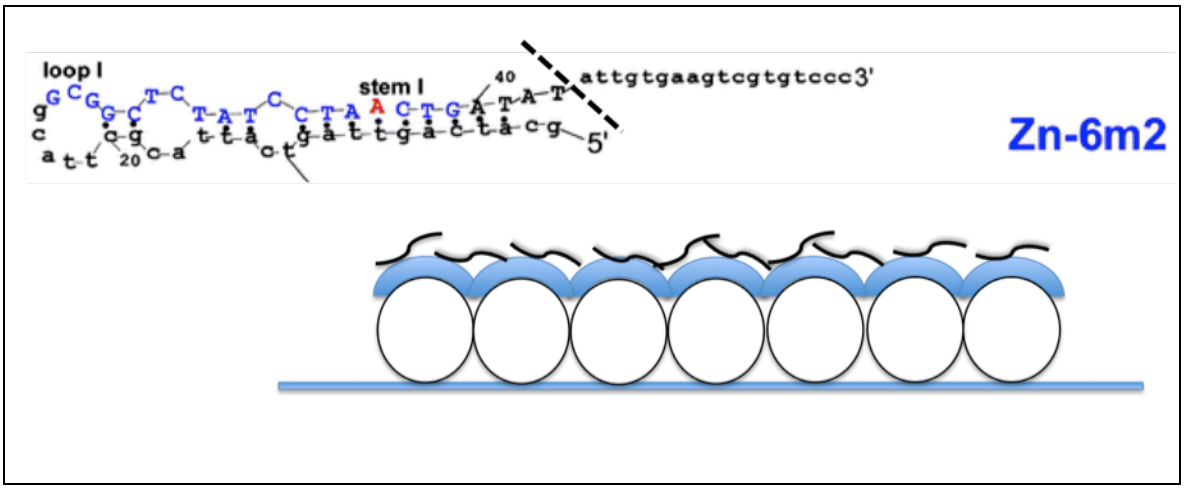

Figure 23. Top is the DNA sequence of aptamer Zn-6m2 in its predicted folded conformation with a dotted line indicating where the aptamer was truncated for this experiment. Bottom is the schematic of the SERS substrate, which consists of a layer of polystyrene beads covered with a thin film of silver (~100 nm). The aptamer was placed on the surface for analysis.

4.2.1 Fabrication of AgFON Substrate

The SERS substrate was created using nanosphere lithography as done previously by Van Duyne et al. (82). Glass slides obtained from Fisher Scientific were cleaned using Piranha (1:3 30%H_2O_2:H_2SO_4) solution and then rendered hydrophilic by using 5:1:1 H_2O:NH_4OH:30% H_2O_2 with sonication for 1 hour. Surfactant-free, white carboxyl substituted polystyrene latex nanospheres with diameters of 390 nm from Duke Scientific, were used undiluted at 2 µl (10%wt/

wt %) and drop coated onto the glass slide. After drying, a thin layer (~100 nm) of silver was thermally deposited on the microsphere mask using the Varian ebeam deposition system. Once the substrates were prepared two samples were tested; one with the aptamer only and the other with the aptamer plus 2 mM zinc ions.

4.2.2 Raman/SERS Results of Zinc Aptamer

The two spectra appear slightly different in the 1300 – 1600 cm^{-1} range as shown in Figure 24. The shifts in wavenumber could be indicators of distortions of the DNA as a result of metal ion binding. A slight shift is evident from 1323 cm^{-1} for the aptamer alone to 1319 cm^{-1} for the aptamer plus zinc. This mode is attributed to the adenine mixed in-plane stretching mode of the 6-member ring. Another adenine ring stretching mode at 733 cm^{-1} shifted to 731 cm^{-1} with zinc present. Zinc interacts preferentially with the N7 of guanine and the N3 of cytosine (83). Therefore, the slight peak shift from 1332 cm^{-1} to 1330 cm^{-1}, which is attributed to C-N stretching in guanine, could be a result of the N7 interaction with the Zn^{2+} ion.

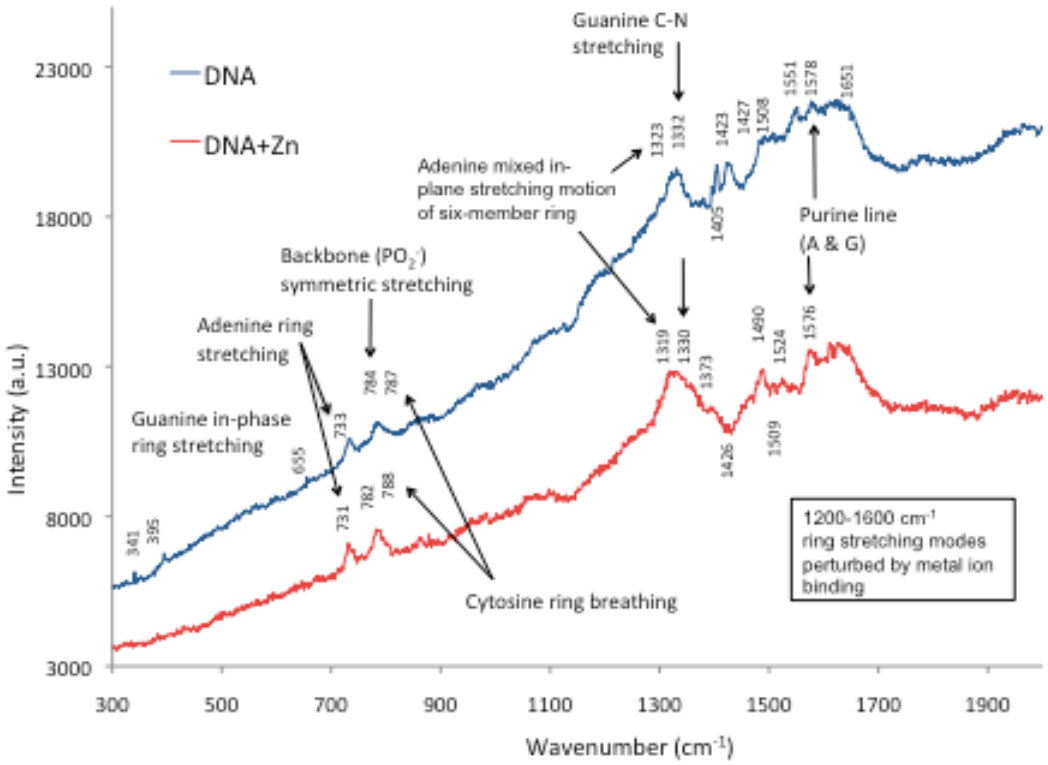

Figure 24. Drop coated sample of unmodified DNA aptamer (blue) and unmodified DNA aptamer + Zn^{2+} (red). Conditions: 8 mW laser power, 120 s exposure time.

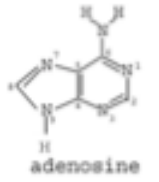
adenosine

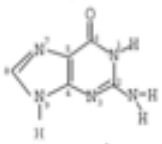
guanine

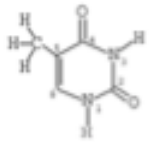
thymine

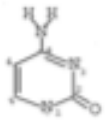
cytosine

Aptamer	Aptamer + Zn^{2+}	Mode designation
655		Guanine in-phase ring stretching of 6-member ring except C_4C_5
733	731	Adenine ring stretching
784	782	Cytosine breathing mode & symmetric stretch of phosphodiester bond
787	788	Cytosine ring breathing mode
	983	Cytosine C_5H breathing mode
1216		Thymine ring & C_5Me stretching
1323	1319	Adenine mixed in-plane stretching mode of 6-member ring
1332	1330	Guanine C_8N_9 & N_7C_8 stretching
1380	1373	Thymine C_5-Me bending
1508	1509	Cytosine N_3C_4 & N_1C_2 stretching
1578	1576	Purine line (A & G)

Table 3. A comparison between the Raman modes of the zinc aptamer alone and the modes produced by the zinc aptamer with zinc. Resolution of Renishaw micro-Raman is 0.8 cm^{-1}.

4.3 DNA Aptamers on Silver Nanorod Array SERS Substrate

AgNR arrays produce enhancement factors of 10^8 without the formation of “hot-spots” (42) Chen *et al*. showed how an array of silver nanoparticles or AgFON, has much greater enhancement where defects occur in the array (10^8 compared with 10^4), but these spaces only account for 0.3% of the excited area (47). The more homogenous surface of the AgNR substrate in terms of enhancement, allows for a more reproducible substrate to be fabricated. Oblique angle deposition is a physical method using a modified E-beam evaporation system developed by the Zhao group at the University of Georgia – Athens (42).

The substrate was created by first applying a titanium adhesion layer, followed by a 200 nm Ag-film base layer onto a glass slide. In order to form silver nanorods, the substrate was positioned such that it formed an oblique angle (4°) relative to the incident vapor. This caused the surface normal of the substrate to be almost parallel with the incident vapor direction. While in this arrangement 2000 nm of Ag was deposited to produce the nanorod array. This process allows for the length and diameter of the nanorods to be controlled,

which in turn means the aspect ratio of the nanorods is controlled. A higher aspect ratio will produce a stronger enhancement effect (42, 84). The enhancement factor is also influenced by the lateral arrangement of the nanorods. The more overlap there was between nanorods, the greater the SERS signal (42, 84, 85). This distance dependent effect, due to the coupling of surface plasmons between nearest-neighbor nanorods, has also been shown with Ag nanoparticles by Schatz *et al.* (86).

4.3.1 Sample Preparation and Equipment Parameters

The TBA is a 15-base sequence of single stranded DNA (ssDNA) comprised of the bases thymine and guanine (5'-GGTTGGTGTGGTTGG-3'). The second sample was a poly-thymine strand 15 bases long. The two samples of ssDNA were prepared for analysis by first being dissolved in Milli-Q water at a concentration of 10 μM. Then 20 μl of sample was pipette onto the SERS substrate and allowed to incubate overnight, allowing the DNA to adsorb to the silver surface. Next the samples were rinsed using Milli-Q water and dried with compressed air. The rinsing step removed any molecules that did not adsorb to the surface of the nanorods, leaving a monolayer. The two sequences were

analyzed using a Renishaw micro-Raman system with an Ar^+ -ion laser (514.5 nm wavelength) and a 50X objective. The spectral resolution is 0.8 cm^{-1}. The laser power measured 23 mW, but this was attenuated using the 1% neutral density (ND) filter to make the laser power at the sample 0.23 mW. The power density for each sample was 13,000 W/cm^2 and the acquisition time was 30 seconds.

4.3.2 Poly-thymine Sequence on AgNR Array

Figure 25 shows the spectrum obtained for a sequence of 15 thymine bases. This spectrum illustrates modes that are characteristic of thymine oligonucleotides, including multiple ring breathing modes at 610, 788, 1007, and 1230 cm^{-1} (87) (87). The line at 610 cm^{-1} could also be attributed to the N3-H wagging in thymine. This line is more prominent in the poly-T sample, where there are a greater number of thymine bases. Table 4 lists the band assignments for the Raman lines seen in Figure 24.

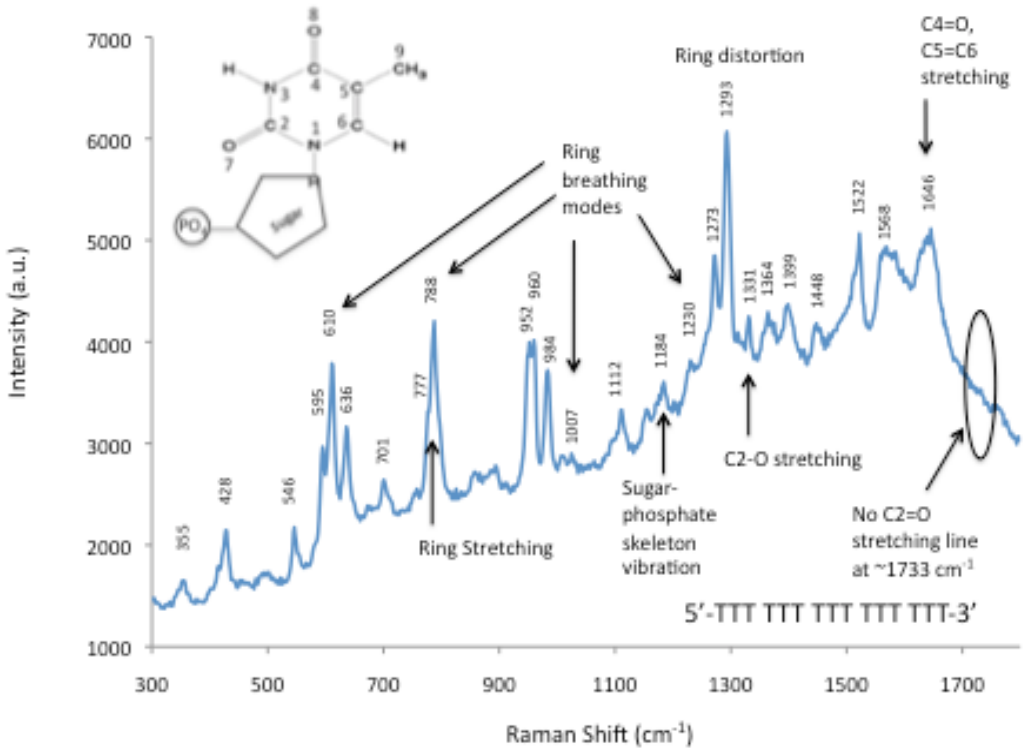

Figure 25. SERS spectrum of single stranded poly-thymine sequence on AgNR array substrate. Upper left is thymine and the deoxyribose sugar and phosphate group, which comprise the DNA backbone.

The sharp peak at 1293 cm^{-1} was attributed to ring distortion and anti-symmetric bending of N3-H and C6-H (88). A vibration form the sugar-phosphate backbone was also identified at 1184 cm^{-1}. In addition to the detection of thymine, the vibrational modes also provide information regarding the adsorption of the molecule to the substrate. The presence of a line for

stretching of the single bond C2-O (1331 cm^{-1}) coupled with the absence of a line for the double bond C2=O indicates that thymine is adsorbing to the nanorods through that atom. Shang *et al.* calculated the C2=O stretching mode for thymine in the gas phase to be 1733 cm^{-1} (87).

SERS Band Position (1/cm)	**Band Assignments**
428, 595	Ring bending
610	N3-H wag, ring breathing
636	N1-C2-O -- N3-C4-O bending, N3-H wag
777	In phase ring stretching
788	Ring breathing
984	Ring distortion, symmetry wag C-H
1007	Ring breathing
1184	Ribose-phosphate skeleton vibration
1230	Ring breathing
1273	Ring stretching, C-H bending
1293	Ring distortion, anti-symmetric bending N3-H, C6-H
1331	C2-O stretching
1364	N3-H, C6-H anti-symmetric bending
1522	In plane ring distortion
1568	C=N stretching
1646	C4=O, C5=C6 stretching

Table 4. List of the prominent peaks for poly-thymine SERS with the associated band assignments.

4.3.3 Thrombin Binding Aptamer on AgNR Array

The TBA contains thymine and guanine bases and the SERS fingerprint is below in Figure 26. The TBA spectrum also shows thymine ring breathing modes at 611, 714, 1007, 1187, 1241, and 1399 cm^{-1}, but also shows ring vibrational modes for guanine at 555 and 652 cm^{-1}. The sharp peak at 805 cm^{-1} is attributed to the guanine bases in the TBA (89) and is not seen in the poly-thymine sample. The sharp peak at 821 cm^{-1} is most likely due to guanine, since it is not shown in the poly-T spectrum. The band assignments for the TBA spectrum are listed in Table 5. Both spectra show a peak for the N3-H/C6-H anti-symmetric bending of thymine at 1364 and 1360 cm^{-1} for poly-T and TBA respectively, but the peak in the TBA spectrum is narrower and at a much higher intensity. There could be contributions from guanine at 1360 cm^{-1} also.

The SERS spectra collected for these two different sequences using AgNR arrays demonstrate how a spectral fingerprint can be used to distinguish between samples. It could also identify or detect targets with known SERS signatures.

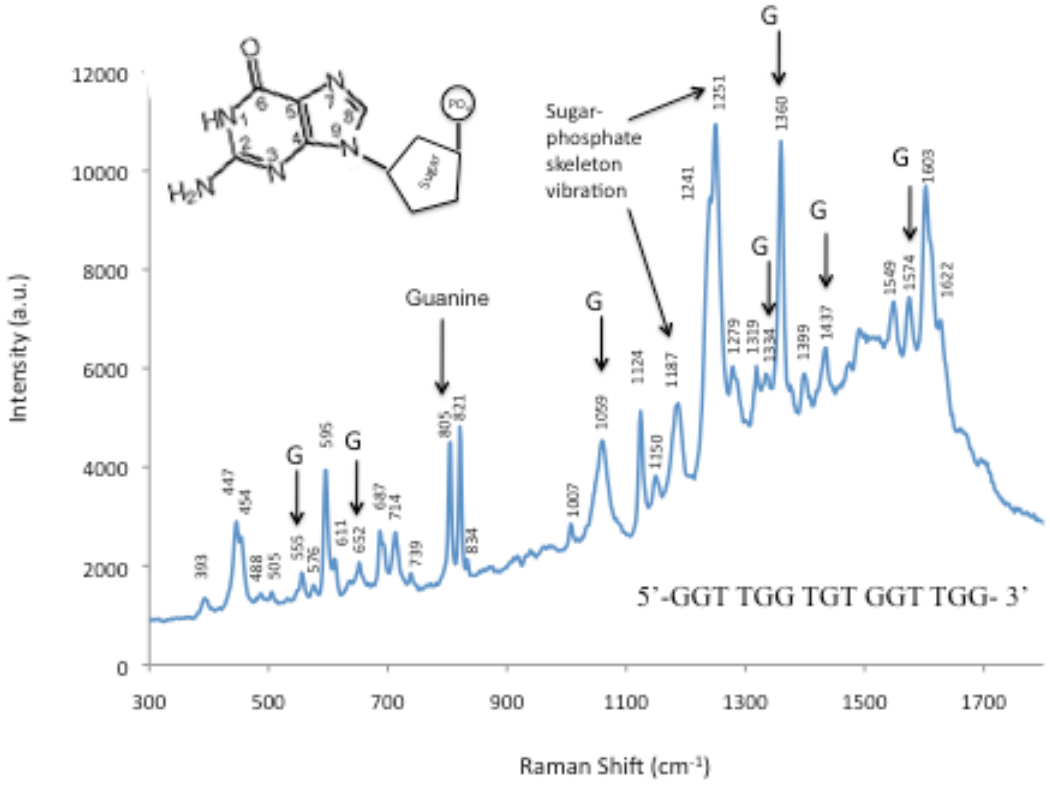

Figure 26. SERS spectrum of DNA sequence TBA. Upper left is the base guanine. Arrows indicate peaks associated with the base guanine.

SERS Band Position (1/cm)	Band Assignments
447	Ring bending
555	Guanine symmetric stretching of 6-membered ring
595	Thymine ring bending
611	Thymine N3-H wag, ring breathing
652	Guanine in phase ring stretching
805	Guanine or phosphate-ribose backbone vibration
1007	Thymine ring breathing
1059	Guanine
1187	Ribose-phosphate skeleton vibration
1251	Ribose-phosphate skeleton vibration
1334	Guanine C8-N9, C8-N7 stretching
1360	Guanine; Thymine in phase asymmetric bending N3-H, C6-H
1399	Guanine C2N3-C2(NH2) stretching
1437	Guanine N1C2-N1C6 stretching
1574	Guanine N3-C4, C4=C5 stretching
1603	Thymine ring distortion, C2=O stretching

Table 5: List of the prominent peaks for TBA SERS with the associated band assignments.

Biosensing can be accomplished using Raman spectroscopy through the use of SERS substrates like the AgNR arrays fabricated with the oblique angle deposition technique discussed above. Moreover, it can be done using very low sample concentrations, which is useful in biomedical applications where samples can be expensive and limited. This also has applications in detecting harmful toxins or viruses (48).

5 PROTEIN DETECTION AND ANALYSIS VIA SERS

Surface-enhanced Raman scattering (SERS) is a phenomenon used to enhance the signal produced by Raman scattering. Raman spectroscopy is a useful tool for sensor development with potential for remote sensing. Raman spectra provide information on the vibrational modes or phonons, between and within molecules. Therefore, you can produce a unique spectral fingerprint for single molecules. The strong localized surface plasmons produced on the surface of the metal by laser excitation enhance the Raman scattering of the molecule near the metal surface. This enhancement is important because Raman cross sections are between 10^{-31} and 10^{-29} cm^2/molecule, compared to fluorescence cross sections which are up to 10^{-16} cm^2/molecule. Furthermore, the Raman signal is proportional to the Raman cross-section, the excitation laser intensity, and the number of molecules in the field of detection. Therefore, by enhancing the signal via SERS, fewer molecules are required for a sufficient signal to be produced. This is especially useful for samples such as saliva, where concentrations of biomarkers are much lower than in blood, for example. In this study the Raman modes of C-reactive protein are studied using silver

nanorod array SERS substrates. A DNA aptamer with affinity for CRP is also measured.

5.1 C-reactive Protein Detection on AgNR Array SERS Substrate

The AgNR array SERS substrates used to study CRP were the same as those described in detail in section 4.3. All three samples were dissolved in deionized water at a concentration of 3.8 uM or 0.5 mg/ml for C-reactive protein. Then 20 μl of sample was pipette onto the SERS substrate and allowed to incubate overnight at 4°C, allowing the sample molecules to adsorb to the silver surface. Next the samples were rinsed using Milli-Q water and dried with compressed air. The rinsing step removed any molecules that did not adsorb to the surface of the nanorods, leaving a monolayer. The samples were analyzed using a Renishaw micro-Raman system with an Ar^+ -ion laser (514.5 nm wavelength) and a 50X objective. The spectral resolution is 0.8 cm^{-1}. The power density for each sample was 13,000 W/cm^2 and the acquisition time was 30 seconds.

The aptamers in this study are potentially adaptable for use in detecting other analytes including those found in human saliva including biomolecules in human saliva that are (a) indicators of past exposure to dangerous substances, and (b) indicators of the onset of diseases in humans. C-reactive protein is an acute-phase protein, which can serve as a biomarker for inflammation and tissue damage (90). Increased levels of CRP have been correlated to cardiovascular disease (CVD) (28). It is present in blood serum as well as saliva. McDevitt et al. have studied its correlation with periodontal disease and developed a lab on a chip assay for detection in saliva samples using antibodies and organic dyes (91). In addition to antibodies that bind to CRP, an aptamer-antibody on-chip sandwich assay (92) and an optical RNA-based aptasensor (29) have been developed. Recently a DNA based aptamer has been selected for CRP (30). This DNA aptamer and its interaction with CRO will be studied using SERS.

Another method for detecting CRP or other biomarkers in saliva that does not require application to a substrate is using Raman spectroscopy. Raman spectroscopy has the potential to be used as a non-invasive method

that does not require sample preparation. By shining a laser in a patient's mouth and detecting the scattered phonons one could identify various molecules. In order to accomplish this type of detection, the Raman modes that are prominent in the target molecule must be identified. For proteins, any modes associated with the amide bond linking each amino acid will be evident. The diagram below shows two common vibrational modes from this bond. The amide 1 mode is mainly a result of the C=O stretching and is typically in the 1630 – 1700 cm^{-1} section. The amide 2 peak is mostly due to N-H wagging and can be found between 1450 and 1550 cm^{-1}.

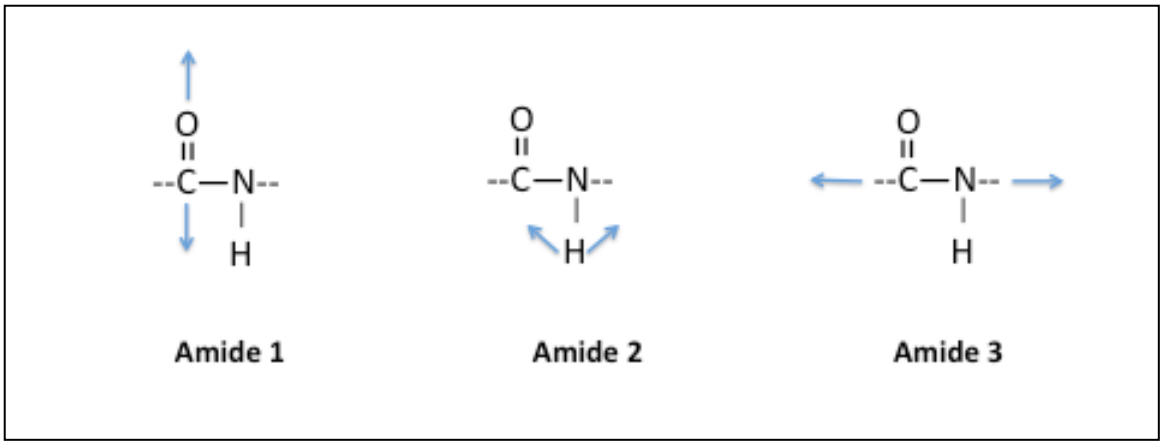

Figure 27. Diagram of the vibrational modes in the amide bond in proteins.

Band Name	Wavenumber Region (cm^{-1})	Vibrational mode
Amide 1	1630 - 1700	C=O stretching
Amide 2	1450 - 1550	N-H bending
Amide 3	1200 - 1400	C-N stretching

Table 6. Amide bands and associated regions and modes.

In the following figure the SERS signature of CRP is shown. The third amide mode is found in the region of 1200 – 1400 cm^{-1}. This is due mainly to the in-phase and out-of-phase N-H bending and C-N stretching (93). In Figure 28 there are multiple peaks in this region, including 1263, 1300, 1332, and 1362 cm^{-1}. The 1332 cm^{-1} peak has been attributed to C-H bending, while the other three modes could be related to the amide bond. Podstawka *et al*. reported an amide 3 mode at 1275 cm^{-1} for a glycine homodipeptide and at 1304 cm^{-1} for leucine. CRP contains approximately 8% glycine and 8% leucine, which make them the third most prevalent amino acids. The peaks at 1263 and 1300 are likely amide 3 modes. The amide 1 mode is a shoulder at 1652 cm^{-1}.

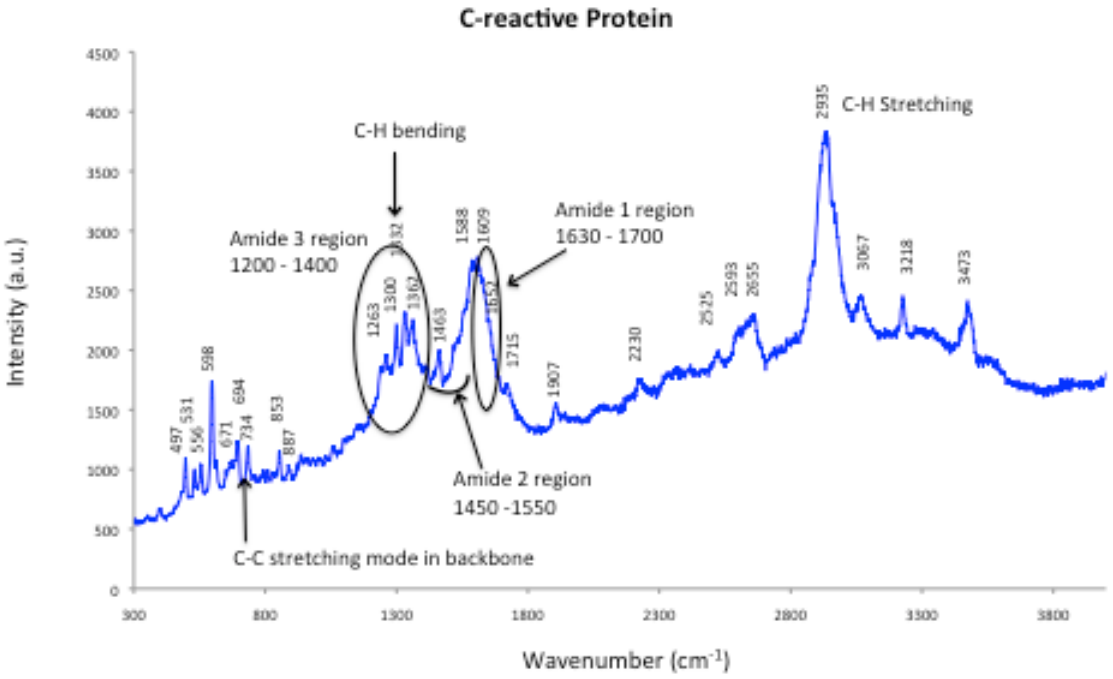

Figure 28: SERS signature of CRP measured on AgNR array substrate.

All amino acids contain a C-H bond and exhibit several C-H stretching vibrational modes. These modes will vary between amino acids as the different R-groups attached to the central carbon atom change. The C-H stretching region is between 2800 and 3100 cm^{-1}. This region is shown in more detail in figure 29.

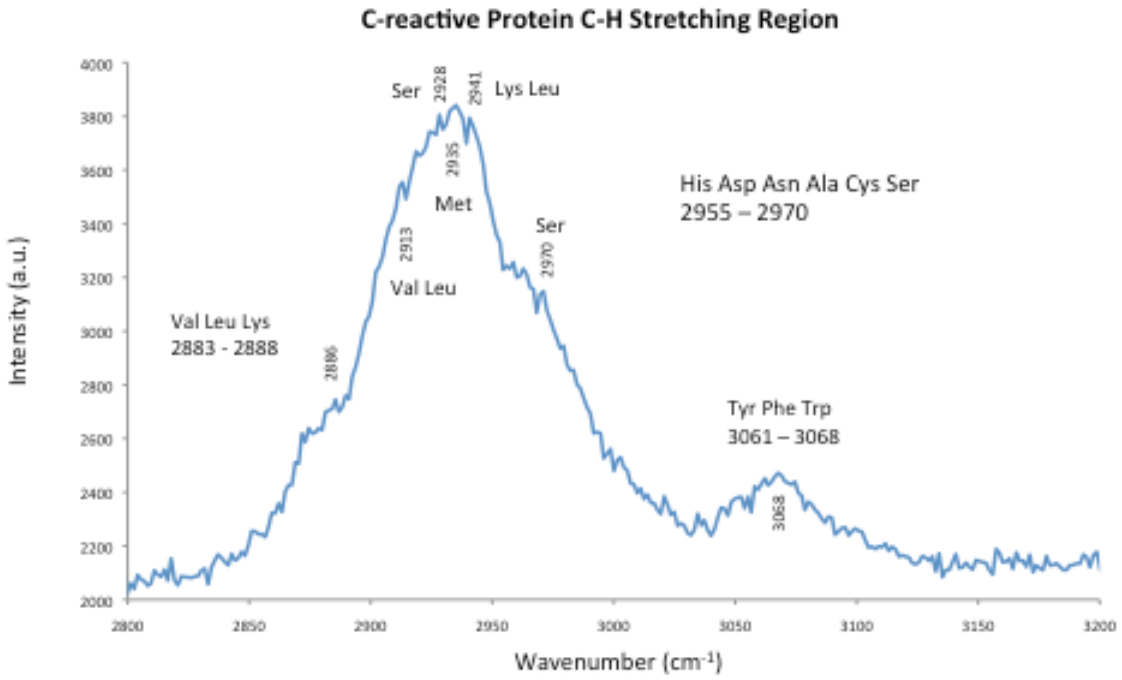

Figure 29: The C-H stretching region for the CRP SERS spectrum indicating which amino acids are contributing to the signal.

Raman Shift (cm^{-1})	Assignment
734	C-C stretching mode in amino acid backbone
1263	Amide 3, C-N stretching
1300	Amide 3, C-N stretching
1332	C-H bending
1362	C_b-H deformation of isopropyl group in valine
1463	Amide 2, mainly N-H bending
1634	Amide I, mainly C=O stretching
2886	C-H stretching Val Leu Lys
2928	C-H stretching Ser
2935	C-H stretching Met
2970	C-H stretching Ser
3068	C-H stretching Tyr Phe Trp

Table 7: Band assignments for SERS spectrum of CRP.

There are 18 serines and 17 valines out of the 183 amino acids that make up CRP. These amino acids, along with glutamine, leucine and glycine

are the most prevalent. There are two peaks with relatively high intensities due to serine (2928 and 2970 cm^{-1}) and two due to valine (2886 and 2913 cm^{-1}), as listed in table 7 (94).

5.2 Anti-C-reactive Protein Aptamer Spectral Studies

The DNA aptamer selected for CRP by Huang *et al.* was studied using surface-enhanced Raman spectroscopy with and without CRP present. The folded structure as predicted by mfold is shown in Figure 30.

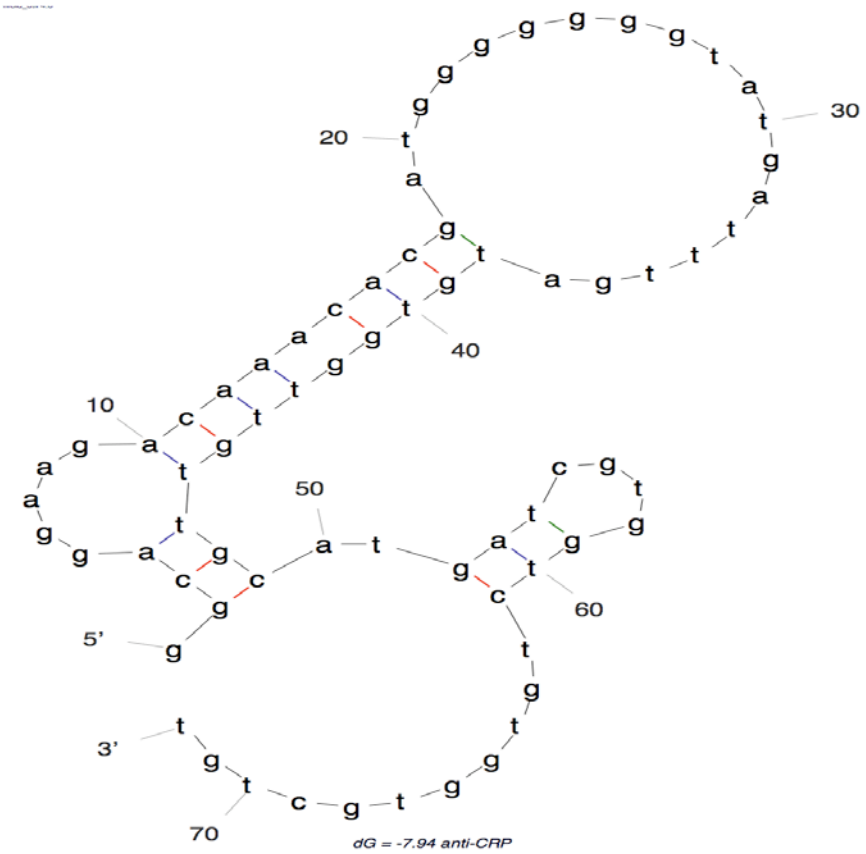

Figure 30: Tertiary structure of the anti-CRP aptamer with the lowest Gibb's free energy, as predicted by mfold.

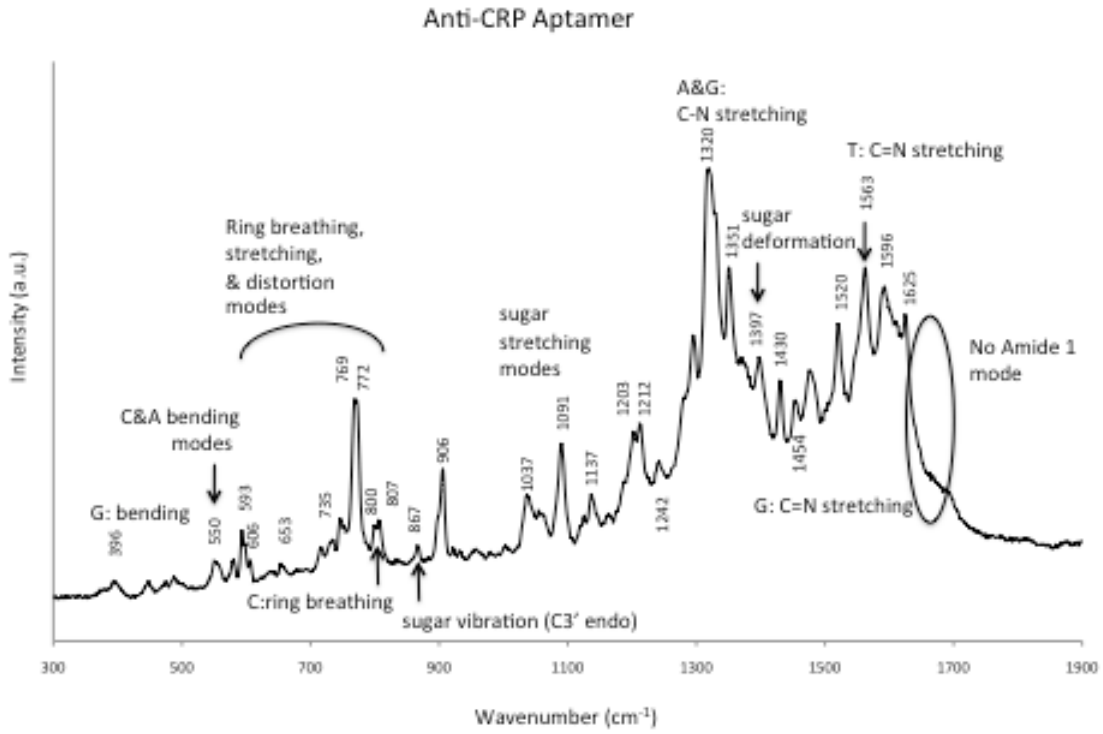

Figure 31: SERS spectrum of anti-CRP aptamer measured on AgNR array substrate. A: adenine, G: guanine, C: cytosine, T: thymine.

The spectrum of the anti-CRP aptamer (Figure 31) contains many sharp peaks for DNA. There is no prominent Amide 1 mode detected. While DNA does have C=O stretching modes in the 1640 – 1680 cm^{-1} region (89), they may be affected by the adsorption to the substrate. There are several sharp peaks in the ring breathing (600 – 800 cm^{-1}) and ring bending (400 – 600 cm^{-1}) regions as outlined in Table 8.

Raman Shift (cm-1)	Band Assignment
396	Guanine C2N14(b)+N9R(b)
550	Cytosine: N1C2N3(b)+C2N3C4(b) Adenine: C5C4N(b)--C2N1C8(b)
581	Thymine N1C2O(b)--C2N3C4(b)
593	Thymine ring bending
606	Thymine N3-H wag, ring breathing
653	Guanine in-phase ring stretching of 6-membered ring except C4C5
716	Thymine ring breathing
735	Adenine ring breathing/stretching
769	Thymine ring distortion
772	Thymine ring breathing/in plane Ring Def
800	Cytosine ring breathing
807	G or Phosphate-deoxyribose backbone vibration
867	sugar vib (C3' endo)
1037	N-sugar stretching
1091	PO4 and sugar stretching
1295	T: Ring distortion, anti-symmetry bend N3-H,C6-H
1320	A&G: C-N stretching
1329 (shoulder)	A&G: C-N stretching
1397	deoxyribosyl (C5'H2) deformation
1454	Guanine C=N stretching
1563	Thymine: C=N stretching
1625	Cytosine: C2=O(s)--C2N3(s)

Table 8. Prominent vibration modes in anti-CRP aptamer SERS spectrum with associated assignment.

A sample of the anti-CRP aptamer with CRP was also analyzed for comparison with the DNA spectrum. Figure 32 below shows both spectra with the DNA with C-reactive protein on the bottom. The DNA with target protein does not show the characteristic ring breathing and stretching modes that are often seen with Raman of DNA. There are modes associated with the sugar phosphate backbone of the DNA in both spectra, but they are somewhat shifted with the CRP bound. Several of the shifted peaks are listed in Table 9.

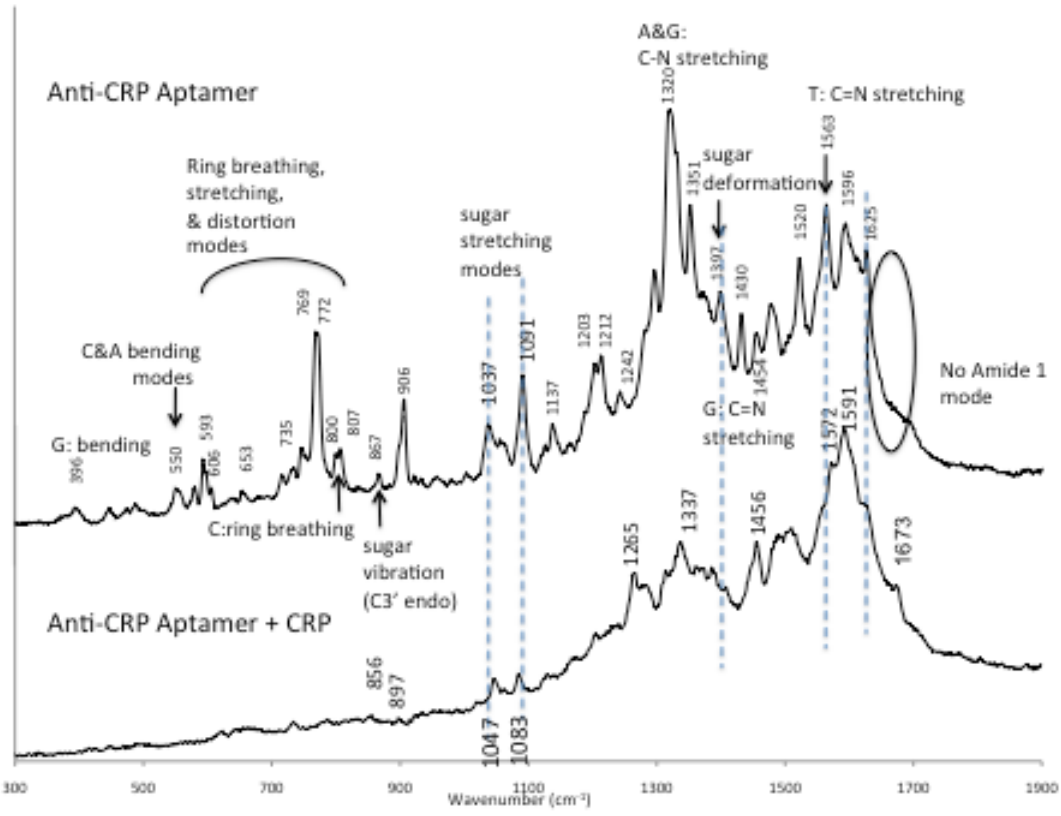

Figure 32: SERS spectra of anti-CRP aptamer and the aptamer with CRP on AgNR array substrate.

Band Designation	DNA Aptamer	Aptamer + CRP
sugar vib (C3' endo)	867	856
N-sugar stretching	1037	1047
PO4 and sugar stretching	1091	1083
deoxyribosyl (C5'H2) deformation	1397	1386
Guanine C=N stretching	1454	1456
Thymine: C=N stretching	1563	1572

Table 9. Peak shifts for the anti-CRP DNA aptamer after interaction with CRP.

6 CONCLUSIONS AND FUTURE DIRECTIONS

6.1 Conclusion

The uses for DNA in nanoscale structures and devices have grown significantly. Beyond just a carrier of genetic information, it has proved a useful and potent molecular beacon for genes, a diverse molecular recognition element in detection schemes as an aptamer, and served as a building block in molecular structures, known as DNA origami. The applications of DNA are not limited to strictly biological conjugations. It has the capacity to interface with synthetic and inorganic materials.

Through the development and testing of optical DNA aptamer-based nanosensors and the study of DNA and proteins through micro-Raman spectroscopy in this research, the following conclusions can be drawn.

1. Semiconductor quantum dots perform as donors in FRET based sensors constructed with DNA aptamers for the detection of heavy metal ions, specifically mercury, lead, cadmium and zinc ions. QDs are larger in diameter than organic fluorophores, but have several advantages including superior

brightness, photostability, symmetric and narrow emission peaks, and a size tunable emission wavelength. They also have a broad excitation range.

2. Gold nanoparticles function in optical sensors in conjunction with QDs as robust and efficient quenchers where organic quenchers have been used.

3. Mercury (II) ions will completely eliminate the quenching of a 10 nM solution of QDs at 55 μM. Above 10 μM the luminescence decreases linearly as the mercury (II) ion concentration increases. Therefore QDs alone cannot detect Hg at the necessary levels of toxicity, given the EPA's drinking water contamination level of 2 ug/L or 10 nM.

4. The increase in lead (II) ions concentration causes the luminescence of QDs (10 nM) to decrease exponentially, but still fluorescing at 900 μM. This effect on QD fluorescence does not occur at the required detection levels for lead where the aptamer-based probe would be needed.

5. The FRET based sensor designed for Hg and Pb detection using a 15-base long aptamer conjugated to a gold nanoparticle and QD was also successfully applied to the detection of Zn and Cd through the use of a 50-base long aptamer. This shows the versatility of this detection platform.

6. The heavy metal ion detection assays were applied to Immobilon-FL (low auto-fluorescence) filter paper on cover slips, which demonstrates the potential for creating disposable coupons for use in a portable hand held device or self administered point of care diagnostics.

7. The low Raman cross section of DNA molecules and proteins can be overcome at low concentrations through the use of surface-enhanced Raman scattering (SERS) substrates, including silver film over nanospheres and silver nanorod arrays. The AgNR arrays produced more distinct peaks at higher intensities.

8. Characteristic Raman modes of several DNA aptamers and C-reactive protein were identified using SERS. These unique signatures have potential in noninvasive label-free detection techniques.

9. Shifts in prominent peaks for DNA aptamers were studied for changes when bound to target. Changes in the sugar-phosphate backbone modes of the anti-CRP aptamer were found after binding to CRP. This spectroscopic technique showed how useful information can be provided for sensor development.

6.2 Future Directions

The future of healthcare is moving toward a more personalized approach. The use of biomarkers like DNA, mRNA, proteins, metabolites, and other compounds or ions play an important role in early detection of disease and risk factor determination. More biomarkers are always being discovered for different disease states and health metrics, just as elevated C-reactive protein levels are used to assess periodontal and heart disease risk. This creates an increased need for diagnostic devices, especially those that are low cost, easy to use and potentially self-administered.

The flexibility and broad target range of aptamers will be very useful for adapting to novel targets as they are discovered, developed, and tested to serve as biomarkers. Aptamers also work well with QDs and gold nanoparticles in FRET based sensor platforms. Another advantage of this sensing platform is that it can be done rapidly. This creates potential for point-of-care diagnostics and home use. If a patient has risk factors for heart disease, tracking specific biomarkers for changes could inform patients and clinicians much earlier of an increased risk for a heart attack.

In order to take the diagnostic aspect of personalized medicine and health monitoring a step further, techniques such as Raman spectroscopy and SERS could be used as label-free and rapid remote sensing techniques. As spectral fingerprints are determined for important biomarkers, especially those in saliva, they can be used for the development of these non-invasive and label-free detection methods. Perhaps a laser could be pointed in a patient's mouth to instantly provide important health information.

REFERENCES

1. Hamaguchi N, Ellington A, Stanton M. Aptamer beacons for the direct detection of proteins. Analytical Biochemistry. 2001;294(2):126-31. doi: 10.1006/abio.2001.5169. PubMed PMID: WOS:000169978800005.
2. Huang CC, Chang HT. Aptamer-based fluorescence sensor for rapid detection of potassium ions in urine. Chemical Communications. 2008(12):1461-3. doi: 10.1039/b718752a. PubMed PMID: WOS:000253983300024.
3. Stojanovic MN, de Prada P, Landry DW. Aptamer-based folding fluorescent sensor for cocaine. Journal of the American Chemical Society. 2001;123(21):4928-31. doi: 10.1021/ja0038171. PubMed PMID: WOS:000168914400007.
4. Baker BR, Lai RY, Wood MS, Doctor EH, Heeger AJ, Plaxco KW. An electronic, aptamer-based small-molecule sensor for the rapid, label-free detection of cocaine in adulterated samples and biological fluids. Journal of the American Chemical Society. 2006;128(10):3138-9. doi: 10.1021/ja056957p. PubMed PMID: WOS:000236035100016.
5. Lai RY, Plaxco KW, Heeger AJ. Aptamer-based electrochemical detection of picomolar platelet-derived growth factor directly in blood serum. Analytical Chemistry. 2007;79(1):229-33. doi: 10.1021/ac061592s. PubMed PMID: WOS:000243143300035.
6. Chen JW, Jiang JH, Gao X, Liu GK, Shen GL, Yu RQ. A New Aptameric Biosensor for Cocaine Based on Surface-Enhanced Raman Scattering Spectroscopy. Chemistry-a European Journal. 2008;14(27):8374-82. doi: 10.1002/chem.200701307. PubMed PMID: WOS:000259913900034.
7. Chen JW, Liu XP, Feng KJ, Liang Y, Jiang JH, Shen GL, Yu RQ. Detection of adenosine using surface-enhanced Raman scattering based on structure-switching signaling aptamer. Biosensors & Bioelectronics. 2008;24(1):66-71. doi: 10.1016/j.bios.2008.03.013. PubMed PMID: WOS:000259425300010.

8. Nutiu R, Li YF. Structure-switching signaling aptamers. Journal of the American Chemical Society. 2003;125(16):4771-8. doi: 10.1021/ja028962o. PubMed PMID: WOS:000182331800035.

9. Zhang ZY, Guo L, Tang JJ, Guo XJ, Xie JW. An aptameric molecular beacon-based "Signal-on" approach for rapid determination of rHuEPO-alpha. Talanta. 2009;80(2):985-90. doi: 10.1016/j.talanta.2009.08.028. PubMed PMID: WOS:000271701900087.

10. Kim GI, Kim KW, Oh MK, Sung YM. The detection of platelet derived growth factor using decoupling of quencher-oligonucleotide from aptamer/quantum dot bioconjugates. Nanotechnology. 2009;20(17). doi: 175503

10.1088/0957-4484/20/17/175503. PubMed PMID: WOS:000264950600013.

11. Alexson D, Chen HF, Cho M, Dutta M, Li Y, Shi P, Raichura A, Ratmadurai D, Parikh S, Stroscio MA, Vasudev M. Semiconductor nanostructures in biological applications. Journal of Physics-Condensed Matter. 2005;17(26):R637-R56. doi: 10.1088/0953-8984/17/26/r01. PubMed PMID: WOS:000231847900002.

12. Ramadurai D, Li Y, Yamanaka T, Geerpuram D, Sankar V, Vasudev M, Alexson D, Shi P, Dutta M, Stroscio MA, Rajh T, Saponjic Z, Kotov N, Tang Z, Xu S, editors. Colloidal quantum dots as optoelectronic elements. Quantum Sensing and Nanophotonic Devices III; 2006; San Jose, CA, USA: SPIE.

13. Ramadurai D, Geerpuram D, Alexson D, Dutta M, Kotov NA, Tang Z, Stroscio MA. Electrical and optical properties of colloidal semiconductor nanocrystals in aqueous environments. Superlattices and Microstructures. 2006;40(1):38-44. doi: 10.1016/j.spmi.2006.03.001. PubMed PMID: WOS:000239649000005.

14. Chen H, Titushkin I, Stroscio M, Cho M. Altered membrane dynamics of quantum dot-conjugated integrins during osteogenic differentiation of human bone marrow derived progenitor cells. Biophysical Journal. 2007;92(4):1399-408. doi: 10.1529/biophysj.106.094896. PubMed PMID: WOS:000244030300033.

15. Shah LS, Clark PA, Moioli EK, Stroscio MA, Mao JJ. Labeling of mesenchymal stem cells by bioconjugated quantum dots. Nano Letters. 2007;7(10):3071-9. doi: 10.1021/nl071547f. PubMed PMID: WOS:000250143400024.

16. Vasudev M, Yamanaka T, Sun K, Li Y, Jianyong Y, Ramadurai D, Strsocio MA, Dutta M, editors. Colloidal Quantum Dots as Optoelectronic Elements. Quantum Sensing and Nanophotonic Devices IV; 2007; San Jose, CA USA: SPIE.

17. Vasudev M, Yamanaka T, Yang J, Li Y, Dutta M, Stroscio MA, editors. Integrated DNA-Nanoparticle Complexes: Synthesis, Electrical and Optical Properties. New Bioanalytical and Biomedical Methods; 2007 6-11 May 2007; Chicago, IL: Curran Associates, Inc.

18. Vasudev M, Yamanaka T, Yang J, Ramadurai D, Stroscio MA, Globus T, Khromova T, Dutta M. Optoelectronic signatures of biomolecules including hybrid nanostructure-DNA ensembles. Ieee Sensors Journal. 2008;8(5-6):743-9. doi: 10.1109/jsen.2008.923183. PubMed PMID: WOS:000258763200046.

19. Ramadurai D, Norton E, Hale J, Garland JW, Stephenson LD, Stroscio MA, Sivananthan S, Kumar A. Fluorescent resonance energy transfer based detection of biological contaminants through hybrid quantum dot-quencher interactions. Iet Nanobiotechnology. 2008;2(2):47-53. doi: 10.1049/iet-nbt:20070033. PubMed PMID: WOS:000256624500003.

20. Vasudev M, Yang J, Jung H-S, Stroscio MA, Dutta M. Integrated Nanostructure-Semiconductor Molecular Complexes as Tools for THz Spectral Studies of DNA. Ieee Sensors Journal. 2010;10(3):524-30. doi: 10.1109/jsen.2009.2037804. PubMed PMID: WOS:000274795400003.

21. Vasudev M, Wu T-C, Biswas S, Dutta M, Stroscio MA, Guthrie S, Reed M, Burris KP, Stewart CN, Jr. Optoelectronic Signatures of DNA-Based Hybrid Nanostructures. Ieee Transactions on Nanotechnology. 2011;10(1):35-43. doi: 10.1109/tnano.2010.2064174. PubMed PMID: WOS:000286933800006.

22. Selid PD, Xu H, Collins EM, Face-Collins MS, Zhao JX. Sensing Mercury for Biomedical and Environmental Monitoring. Sensors. 2009;9(7):5446-59. doi: 10.3390/s90705446. PubMed PMID: WOS:000268317000022.

23. Kägi JHR, Nordberg M, American Society of Biological Chemists. Metallothionein. Basel ; Boston: Birkhauser; 1979. 378 p. p.

24. Tyagi S, Bratu DP, Kramer FR. Multicolor molecular beacons for allele discrimination. Nature Biotechnology. 1998;16(1):49-53. doi: 10.1038/nbt0198-49. PubMed PMID: WOS:000071306000028.

25. Sigel H. Reactivity of coordination compounds. New York ; Basel: M. Dekker; 1976. xiii, 401 p. p.

26. McElroy JA, Bryda EC, McKay SD, Schnabel RD, Taylor JF. Genetic Variation at a Metallothionein 2A Promoter Single-Nucleotide Polymorphism in White and Black Females in Midwestern United States. Journal of Toxicology and Environmental Health-Part a-Current Issues. 2010;73(19):1283-7. doi: Pii 925758858

10.1080/15287394.2010.485067. PubMed PMID: WOS:000281078300001.

27. Wong DT. Salivary diagnostics. American Scientist. 2008;96(1):37-43. doi: 10.1511/2008.69.3669. PubMed PMID: WOS:000251467100024.

28. Pepys MB, Hirschfield GM. C-reactive protein: a critical update. Journal of Clinical Investigation. 2003;111(12):1805-12. doi: 10.1172/jci18921. PubMed PMID: WOS:000183623600002.

29. Bini A, Centi S, Tombelli S, Minunni M, Mascini M. Development of an optical RNA-based aptasensor for C-reactive protein. Analytical and Bioanalytical Chemistry. 2008;390(4):1077-86. doi: 10.1007/s00216-007-1736-7. PubMed PMID: WOS:000252918100010.

30. Huang C-J, Lin H-I, Shiesh S-C, Lee G-B. Integrated microfluidic system for rapid screening of CRP aptamers utilizing systematic evolution of ligands by exponential enrichment (SELEX). Biosensors & Bioelectronics. 2010;25(7):1761-6. doi: 10.1016/j.bios.2009.12.029. PubMed PMID: WOS:000275978700034.

31. Zhang XY, Young MA, Lyandres O, Van Duyne RP. Rapid detection of an anthrax biomarker by surface-enhanced Raman spectroscopy. Journal of the American Chemical Society. 2005;127(12):4484-9. doi: 10.1021/ja043623b. PubMed PMID: WOS:000227895500069.

32. Garcon G, Leleu B, Marez T, Zerimech F, Jean-Marie HD, Daniel FB, Shirali P. Biomonitoring of the adverse effects induced by the chronic

exposure to lead and cadmium on kidney function: Usefulness of alpha-glutathione S-transferase. Science of the Total Environment. 2007;377(2-3):165-72. doi: 10.1016/j.scitotenv.2007.02.002. PubMed PMID: WOS:000247024600005.

33. Brenneman K, Sen B, Stroscio MA, Dutta M. Aptamer-based optical bionano sensor for mercury(II) ions. Nanotechnology Materials and Devices Conference (NMDC), 2010 IEEE; 12-15 Oct. 2010; Monterey, CA, USA2010. p. 221-4.

34. Rajendran M, Ellington AD. Selection of fluorescent aptamer beacons that light up in the presence of zinc. Analytical and Bioanalytical Chemistry. 2008;390(4):1067-75. doi: 10.1007/s00216-007-1735-8. PubMed PMID: WOS:000252918100009.

35. Ellis KJ, Yuen K, Yasumura S, Cohn SH. DOSE - RESPONSE ANALYSIS OF CADMIUM IN MAN - BODY BURDEN VS KIDNEY DYSFUNCTION. Environmental Research. 1984;33(1):216-26. doi: 10.1016/0013-9351(84)90018-5. PubMed PMID: WOS:A1984SC65800017.

36. Fosmire GJ. ZINC TOXICITY. American Journal of Clinical Nutrition. 1990;51(2):225-7. PubMed PMID: WOS:A1990CP70500017.

37. Khan DA, Qayyum S, Saleem S, Khan FA. Evaluation of lead body burden in occupational workers by lead mobilization test. JPMA The Journal of the Pakistan Medical Association. 2009;59(6):350-4. PubMed PMID: MEDLINE:19534366.

38. Organization WH. Mercury in Drinking-waterBackground document for development of WHO *Guidelines for Drinking-water Quality*. 2005.

39. Johnsson C, Schutz A, Sallsten G. Impact of consumption of freshwater fish on mercury levels in hair, blood, urine, and alveolar air. Journal of Toxicology and Environmental Health-Part a-Current Issues. 2005;68(2):129-40. doi: 10.1080/15287390590885992. PubMed PMID: WOS:000226256200004.

40. Rikans LE, Yamano T. Mechanisms of cadmium-mediated acute hepatotoxicity. Journal of Biochemical and Molecular Toxicology. 2000;14(2):110-7. doi: 10.1002/(sici)1099-0461(2000)14:2<110::aid-jbt7>3.0.co;2-j. PubMed PMID: WOS:000084522500007.

41. Wong DT. Salivary diagnostics powered by nanotechnologies, proteomics and genomics. Journal of the American Dental Association. 2006;137(3):313-21. PubMed PMID: WOS:000236081800022.

42. Chaney SB, Shanmukh S, Dluhy RA, Zhao YP. Aligned silver nanorod arrays produce high sensitivity surface-enhanced Raman spectroscopy substrates. Applied Physics Letters. 2005;87(3):3. doi: 031908

10.1063/1.1988980. PubMed PMID: WOS:000230596000020.

43. Willets KA, Van Duyne RP. Localized surface plasmon resonance spectroscopy and sensing. Annual Review of Physical Chemistry. Palo Alto: Annual Reviews; 2007. p. 267-97.

44. Shafer-Peltier KE, Haynes CL, Glucksberg MR, Van Duyne RP. Toward a glucose biosensor based on surface-enhanced Raman scattering. Journal of the American Chemical Society. 2003;125(2):588-93. doi: 10.1021/ja028255v. PubMed PMID: WOS:000180311800054.

45. Yonzon CR, Stuart DA, Zhang XY, McFarland AD, Haynes CL, Van Duyne RP. Towards advanced chemical and biological nanosensors - An overview. Talanta. 2005;67(3):438-48. doi: 10.1016/j.talanta.2005.06.039. PubMed PMID: WOS:000231936400002.

46. Yonzon CR, Jeoungf E, Zou SL, Schatz GC, Mrksich M, Van Duyne RP. A comparative analysis of localized and propagating surface plasmon resonance sensors: The binding of concanavalin a to a monosaccharide functionalized self-assembled monolayer. Journal of the American Chemical Society. 2004;126(39):12669-76. doi: 10.1021/ja047118q. PubMed PMID: WOS:000224219900088.

47. Chien F-C, Huang WY, Shiu J-Y, Kuo CW, Chen P. Revealing the spatial distribution of the site enhancement for the surface enhanced Raman scattering on the regular nanoparticle arrays. Optics Express. 2009;17(16):13974-81. PubMed PMID: WOS:000268843700074.

48. Shanmukh S, Jones L, Driskell J, Zhao Y, Dluhy R, Tripp RA. Rapid and sensitive detection of respiratory virus molecular signatures using a silver nanorod array SERS substrate. Nano Letters. 2006;6(11):2630-6. doi: 10.1021/nl061666f. PubMed PMID: WOS:000241856700043.

49. Li J, Fattal D, Li Z. Plasmonic optical antennas on dielectric gratings with high field enhancement for surface enhanced Raman spectroscopy. Applied Physics Letters. 2009;94(26). doi: 263114

10.1063/1.3168498. PubMed PMID: WOS:000267697300051.

50. Lee YH, Dai S, Young JP. Silver-doped sol-gel films as the substrate for surface-enhanced Raman scattering. Journal of Raman Spectroscopy. 1997;28(8):635-9. doi: 10.1002/(sici)1097-4555(199708)28:8<635::aid-jrs152>3.0.co;2-0. PubMed PMID: WOS:A1997XY94700012.

51. Huang Y, Yang Y, Chen Z, Li X, Nogami M. Fabricating Au-Ag core-shell composite films for surface-enhanced Raman scattering. Journal of Materials Science. 2008;43(15):5390-3. doi: 10.1007/s10853-008-2793-9. PubMed PMID: WOS:000257751000044.

52. Kahraman M, Aydin O, Culha M. Oligonucleotide-Mediated Au-Ag Core-Shell Nanoparticles. Plasmonics. 2009;4(4):293-301. doi: 10.1007/s11468-009-9105-3. PubMed PMID: WOS:000272121800007.

53. Sharma SK. New trends in telescopic remote Raman spectroscopic instrumentation. Spectrochimica Acta Part a-Molecular and Biomolecular Spectroscopy. 2007;68(4):1008-22. doi: 10.1016/j.saa.2007.06.047. PubMed PMID: WOS:000251747000002.

54. Ellington AD, Szostak JW. INVITRO SELECTION OF RNA MOLECULES THAT BIND SPECIFIC LIGANDS. Nature. 1990;346(6287):818-22. doi: 10.1038/346818a0. PubMed PMID: WOS:A1990DW48800045.

55. Tuerk C, Gold L. SYSTEMATIC EVOLUTION OF LIGANDS BY EXPONENTIAL ENRICHMENT - RNA LIGANDS TO BACTERIOPHAGE-T4 DNA-POLYMERASE. Science. 1990;249(4968):505-10. doi: 10.1126/science.2200121. PubMed PMID: WOS:A1990DR81100032.

56. Lee J-O, So H-M, Jeon E-K, Chang H, Won K, Kim YH. Aptamers as molecular recognition elements for electrical nanobiosensors. Analytical and Bioanalytical Chemistry. 2008;390(4):1023-32. doi: 10.1007/s00216-007-1643-y. PubMed PMID: WOS:000252918100004.

57. Stoltenburg R, Reinemann C, Strehlitz B. SELEX-A (r)evolutionary method to generate high-affinity nucleic acid ligands. Biomolecular

Engineering. 2007;24(4):381-403. doi: 10.1016/j.bioeng.2007.06.001. PubMed PMID: WOS:000250243900003.

58. Zuker M. Mfold web server for nucleic acid folding and hybridization prediction. Nucleic Acids Research. 2003;31(13):3406-15. doi: 10.1093/nar/gkg595. PubMed PMID: WOS:000183832900029.

59. Ruedas-Rama MJ, Hall EAH. Azamacrocycle Activated Quantum Dot for Zinc Ion Detection. Analytical Chemistry. 2008;80(21):8260-8. doi: 10.1021/ac801396y. PubMed PMID: WOS:000260567000050.

60. Alivisatos AP. Perspectives on the physical chemistry of semiconductor nanocrystals. Journal of Physical Chemistry. 1996;100(31):13226-39. doi: 10.1021/jp9535506. PubMed PMID: WOS:A1996VA59500038.

61. Klarreich E. Biologists join the dots. Nature. 2001;413(6855):450-2. doi: 10.1038/35097256. PubMed PMID: WOS:000171340500014.

62. Clapp AR, Medintz IL, Uyeda HT, Fisher BR, Goldman ER, Bawendi MG, Mattoussi H. Quantum dot-based multiplexed fluorescence resonance energy transfer. Journal of the American Chemical Society. 2005;127(51):18212-21. doi: 10.1021/ja054630i. PubMed PMID: WOS:000234258700052.

63. Hines MA, Guyot-Sionnest P. Synthesis and characterization of strongly luminescing ZnS-Capped CdSe nanocrystals. Journal of Physical Chemistry. 1996;100(2):468-71. doi: 10.1021/jp9530562. PubMed PMID: WOS:A1996TP94200009.

64. Chan WCW, Nie SM. Quantum dot bioconjugates for ultrasensitive nonisotopic detection. Science. 1998;281(5385):2016-8. doi: 10.1126/science.281.5385.2016. PubMed PMID: WOS:000076161800052.

65. Dubertret B, Calame M, Libchaber AJ. Single-mismatch detection using gold-quenched fluorescent oligonucleotides. Nature Biotechnology. 2001;19(4):365-70. doi: 10.1038/86762. PubMed PMID: WOS:000167940700027.

66. Selvin PR. The renaissance of fluorescence resonance energy transfer. Nature Structural Biology. 2000;7(9):730-4. doi: 10.1038/78948. PubMed PMID: WOS:000089078500011.

67. Lakowicz JR. Principles of Fluorescence Spectroscopy. 3rd ed. New York: Springer; 2006.

68. Jennings TL, Schlatterer JC, Singh MP, Greenbaum NL, Strouse GF. NSET molecular beacon analysis of hammerhead RNA substrate binding and catalysis. Nano Letters. 2006;6(7):1318-24. doi: 10.1021/nl052458a. PubMed PMID: WOS:000238973100003.

69. Yun CS, Javier A, Jennings T, Fisher M, Hira S, Peterson S, Hopkins B, Reich NO, Strouse GF. Nanometal surface energy transfer in optical rulers, breaking the FRET barrier. Journal of the American Chemical Society. 2005;127(9):3115-9. doi: 10.1021/ja043940i. PubMed PMID: WOS:000227479600069.

70. Pons T, Medintz IL, Sapsford KE, Higashiya S, Grimes AF, English DS, Mattoussi H. On the quenching of semiconductor quantum dot photoluminescence by proximal gold nanoparticles. Nano Letters. 2007;7(10):3157-64. doi: 10.1021/nl071729+. PubMed PMID: WOS:000250143400039.

71. Liu C-W, Huang C-C, Chang H-T. Highly Selective DNA-Based Sensor for Lead(II) and Mercury(II) Ions. Analytical Chemistry. 2009;81(6):2383-7. doi: 10.1021/ac8022185. PubMed PMID: WOS:000264142000046.

72. Fu XB, Qu F, Li NB, Luo HQ. A label-free thrombin binding aptamer as a probe for highly sensitive and selective detection of lead(II) ions by a resonance Rayleigh scattering method. Analyst. 2012;137(5):1097-9. doi: 10.1039/c2an15980e. PubMed PMID: WOS:000300038400007.

73. Wu C-S, Oo MKK, Fan X. Highly Sensitive Multiplexed Heavy Metal Detection Using Quantum-Dot-Labeled DNAzymes. Acs Nano. 2010;4(10):5897-904. doi: 10.1021/nn1021988. PubMed PMID: WOS:000283453700056.

74. Ono A, Togashi H. Highly selective oligonucleotide-based sensor for mercury(II) in aqueous solutions. Angewandte Chemie-International Edition. 2004;43(33):4300-2. doi: 10.1002/anie.200454172. PubMed PMID: WOS:000223603600009.

75. Vaz JLL, Atbir T, Albourine A, PetitRamel M. Binary and ternary interactions of mercury(II) with seven pyrimidines and

ethylenediaminetetraacetic acid. Journal of Chemical Research-S. 1997(8):280-1. doi: 10.1039/a703085a. PubMed PMID: WOS:A1997YC93700008.

76. Bruchez M, Moronne M, Gin P, Weiss S, Alivisatos AP. Semiconductor nanocrystals as fluorescent biological labels. Science. 1998;281(5385):2013-6. doi: 10.1126/science.281.5385.2013. PubMed PMID: WOS:000076161800051.

77. Liu W, Fu Y, Zheng B, Cheng S, Li W, Lau TC, Liang HJ. Kinetics and Mechanism of Conformational Changes in a G-Quadruplex of Thrombin-Binding Aptamer Induced by Pb2+. Journal of Physical Chemistry B. 2011;115(44):13051-6. doi: 10.1021/jp2074489. PubMed PMID: WOS:000296394100043.

78. Zarkowsky D, Lamoreaux L, Chattopadhyay P, Koup RA, Perfetto SP, Roederer M. Heavy Metal Contaminants Can Eliminate Quantum Dot Fluorescence. Cytometry Part A. 2011;79A(1):84-9. doi: 10.1002/cyto.a.20986. PubMed PMID: WOS:000285980700011.

79. Chen YF, Rosenzweig Z. Luminescent CdS quantum dots as selective ion probes. Analytical Chemistry. 2002;74(19):5132-8. doi: 10.1021/ac0258251. PubMed PMID: WOS:000178418100046.

80. West PR, Ishii S, Naik GV, Emani NK, Shalaev VM, Boltasseva A. Searching for better plasmonic materials. Laser & Photonics Reviews. 2010;4(6):795-808. doi: 10.1002/lpor.200900055. PubMed PMID: WOS:000284017900007.

81. Moskovits M. Surface-enhanced Raman spectroscopy: a brief retrospective. Journal of Raman Spectroscopy. 2005;36(6-7). doi: 10.1002/jrs.1362. PubMed PMID: WOS:000230829200004.

82. Zhang X, Yonzon CR, Van Duyne RP. Nanosphere lithography fabricated plasmonic materials and their applications. Journal of Materials Research. 2006;21(5):1083-92. doi: 10.1557/jmr.2006.0136. PubMed PMID: WOS:000237584600001.

83. Duguid J, Bloomfield VA, Benevides J, Thomas GJ. RAMAN SPECTRAL STUDIES OF NUCLEIC-ACIDS .44. RAMAN-SPECTROSCOPY OF DNA-METAL COMPLEXES .1. INTERACTIONS AND

CONFORMATIONAL EFFECTS OF THE DIVALENT-CATIONS - MG, CA, SR, BA, MN, CO, NI, CU, PD, AND CD. Biophysical Journal. 1993;65(5):1916-28. PubMed PMID: WOS:A1993MF32100023.

84. Yang Y, Xiong LM, Shi JL, Nogami M. Aligned silver nanorod arrays for surface-enhanced Raman scattering. Nanotechnology. 2006;17(10):2670-4. doi: 10.1088/0957-4484/17/10/038. PubMed PMID: WOS:000238229100038.

85. Liu YJ, Zhang ZY, Dluhy RA, Zhao YP. The SERS response of semiordered Ag nanorod arrays fabricated by template oblique angle deposition. Journal of Raman Spectroscopy. 2010;41(10):1112-8. doi: 10.1002/jrs.2567. PubMed PMID: ISI:000284023100004.

86. Zhao LL, Kelly KL, Schatz GC. The extinction spectra of silver nanoparticle arrays: Influence of array structure on plasmon resonance wavelength and width. Journal of Physical Chemistry B. 2003;107(30). doi: 10.1021/jp034235j. PubMed PMID: WOS:000184357100019.

87. Shang Z-G, Ting DN, Wong YT, Tan YC, Ying B, Mo Y-J. A study of DFT and surface enhanced Raman scattering in silver colloids for thymine. Journal of Molecular Structure. 2007;826(1). doi: 10.1016/j.molstruc.2006.05.007. PubMed PMID: WOS:000243822000008.

88. Shang Z, Gao Y, Jia T, Mo Y. Vibrational modes study of thymine on the surface of copper electrode using SERS-measurement and the DFT method. Journal of Molecular Structure. 2009;930(1-3). doi: 10.1016/j.molstruc.2009.04.038. PubMed PMID: WOS:000268403100011.

89. Otto C, Vandentweel TJJ, Demul FFM, Greve J. SURFACE-ENHANCED RAMAN-SPECTROSCOPY OF DNA BASES. Journal of Raman Spectroscopy. 1986;17(3). doi: 10.1002/jrs.1250170311. PubMed PMID: WOS:A1986C822400010.

90. Pepys MB, Baltz ML. ACUTE PHASE PROTEINS WITH SPECIAL REFERENCE TO C-REACTIVE PROTEIN AND RELATED PROTEINS (PENTAXINS) AND SERUM AMYLOID A-PROTEIN. Advances in Immunology. 1983;34:141-212. doi: 10.1016/s0065-2776(08)60379-x. PubMed PMID: WOS:A1983RQ28800005.

91. Christodoulides N, Mohanty S, Miller CS, Langub MC, Floriano PN, Dharshan P, Ali MF, Bernard B, Romanovicz D, Anslyn E, Fox PC, McDevitt JT. Application of microchip assay system for the measurement of C-reactive protein in human saliva. Lab on a Chip. 2005;5(3):261-9. doi: 10.1039/b414194f. PubMed PMID: WOS:000227186500004.

92. Pultar J, Sauer U, Domnanich P, Preininger C. Aptamer-antibody on-chip sandwich immunoassay for detection of CRP in spiked serum. Biosensors & Bioelectronics. 2009;24(5):1456-61. doi: 10.1016/j.bios.2008.08.052. PubMed PMID: WOS:000263199800066.

93. Podstawka E, Ozaki Y, Proniewicz LM. Part I: Surface-enhanced Raman spectroscopy investigation of amino acids and their homodipeptides adsorbed on colloidal silver. Applied Spectroscopy. 2004;58(5):570-80. doi: 10.1366/000370204774103408. PubMed PMID: WOS:000221415000013.

94. Howell NK, Arteaga G, Nakai S, Li-Chan ECY. Raman spectral analysis in the C-H stretching region of proteins and amino acids for investigation of hydrophobic interactions. Journal of Agricultural and Food Chemistry. 1999;47(3). doi: 10.1021/jf981074l. PubMed PMID: WOS:000079227300024.

95. Chiang C-K, Huang C-C, Liu C-W, Chang H-T. Oligonucleotide-based fluorescence probe for sensitive and selective detection of mercury(II) in aqueous solution. Analytical Chemistry. 2008;80(10):3716-21. doi: 10.1021/ac800142k. PubMed PMID: WOS:000255871500025.

CURRICULUM VITA

EDUCATION

- Ph.D. Bioengineering, Aug 2013
  University of Illinois at Chicago, Chicago, IL
  Advisors: Michael A. Stroscio, Ph.D.
  Mitra Dutta, Ph.D.
  Thesis: DNA-based nanoconstructs for detection of ions and biomolecules with related Raman/SERS signature studies

- B.S. Biological & Food Process Engineering, Dec 2003
  Purdue University, West Lafayette, IN
  Research Assistant – Jenna Rickus, Ph.D., July 2003 – April 2004
    - Designed and conducted experiments using fiber optic equipment contributing to acquisition of a $278,000 grant
    - Managed research and logistics for purchase of $4K piece of lab equipment needed to further investigation
    - Developed calibration curve for measuring ATP concentration based on bioluminescent reaction and luminometer
    - Utilized sol-gel technique to immobilize enzymes and reactants for biosensor development

PROFESSIONAL EXPERIENCE

UIC OFFICE OF ANIMAL CARE & INSTITUTIONAL BIOSAFETY, Chicago, IL
Graduate Assistant, Jun 2012 – Present

- Clerical work, including processing of animal research protocol submissions and preparing meeting paperwork

VISCOFAN USA, INC., Montgomery, AL
Project Manager / Cellulose Product Manager, Jun 2006 – Aug 2008

- Coordinated sample production, field testing, result reporting, and next steps for raw material conversion
- Aided in development of database system for managing product related requests from sales team

- Facilitated qualification of new casing through work on test design, data collection, cook tests, and analysis

On-Site Project Manager at Sara Lee, Apr 2004 – Jun 2008

- Resolved customer complaint via data collection and analysis, which lead to change in size of equipment part
- Provided product samples for commercialization of new products and oversaw testing at customer locations
- Ensured projects were handled via customer's Product Change Management process
- Reported status of projects to customer in weekly reviews and compiled monthly sales and inventory reports

KRAFT FOODS, INC., Glenview, IL

Engineering Co-op, Jan 2000 - Dec 2000

- Helped to eliminate raw material cost variance of $125M annually for Miracle Whip
- Improved product quality of Miracle Whip by optimizing starch cook temperature based on microscopy results, viscosity data, and product performance in applications
- Recommended calcium source for fortification of fat free cottage cheese by presenting findings to business team
- Presented product evaluation results for different ingredients to technical panel
- Trained co-workers on instrument operation and drafted instructions for rapid measurements of moisture and fat
- Coordinated sample collection and analysis with plant personnel in order to calibrate near-infrared instrument

PEER REVIEWED PUBLICATIONS

Journal Papers

Kimber L. Brenneman, Shripriya Poduri, Michael A. Stroscio, *Fellow IEEE*, and Mitra Dutta, *Fellow IEEE,* Optical Detection of Lead (II) Ions Using DNA-

based Nanosensor. *IEEE Sensors Journal,* vol.13, no.5, pp.1783-1786, May 2013.

Book Chapters

Zhiping Wang, Nanzhu Zhang, **Kimber Brenneman**, Tsai Chin Wu, Hyeson Jung, Sushmita Biswas, Kitt Reinhardt, Sicheng Liao, Michael A. Stroscio, and Mitra Dutta, Optoelectronic Applications of Colloidal Quantum Dots. *Lecture Notes in Nanoscale Science and Technology,* 1, Vol. 13*, Quantum Dot Devices* pp.351-367, 2012.

Conference Proceedings

Kimber L. Brenneman, Xenia Meshik, Ke Xu, Justin Abell, Yiping Zhao, Mitra Dutta, and Michael A. Stroscio, Surface-Enhanced Raman Spectroscopy Study of Single Stranded DNA Sequences on Silver Nanorod Array. PHONONS 2012, July 8-12, 2012, Ann Arbor, Michigan. Paper ID 161 AIP Conf. Proc. Vol. 1506, pp. 53-56, 2012; doi:http://dx.doi.org/10.1063/1.4772525

Ke Xu, Justin Abell, Yiping Zhao, Jun Qian**, Kimber Brenneman,** Xenia Meshik, Mitra Dutta, Michael Stroscio, Surface-Enhanced Raman Spectroscopy as a Tool for Characterizing Nanostructures Containing Molecular Components, PHONONS 2012, July 8-12, 2012, Ann Arbor, Michigan. Paper ID 40 AIP Conf. Proc. 1506, pp. 57-61 (2011); doi:http://dx.doi.org/10.1063/1.4772526

Xenia Meshik**, Kimber Brenneman,** Ke Xu, Justin Abell, Yiping Zhao, Mitra Dutta, Michael Stroscio, Surface-Enhanced Raman Spectroscopy Signatures of an RNA Molecule: An Aptamer that Binds to the $\alpha_v\beta_3$ Integrin, PHONONS 2012, July 8-12, 2012, Ann Arbor, Michigan. Paper ID 61; AIP Conf. Proc. 1506, pp. 49-52 (2011); doi:http://dx.doi.org/10.1063/1.4772524

Kimber L. Brenneman, Banani Sen, Michael A. Stroscio, and Mitra Dutta, Aptamer-based Optical Bionano Sensor for Mercury (II) Ions. *IEEE Nanotechnology Materials and Device Conference* Proceedings, 2010.

Encyclopedia Articles

Mitra Dutta, Michael A. Stroscio, Jun Qian, TsaiChin Wu, **Kimber Brenneman**, Banani Sen, Shripriya Poduri, Ke Xu, Xenia Meshik, Saadia M. Ranginwala, Pitamber Shukla, and Nanzhu Zhang, Nanosensors Based on DNA and RNA Aptamers and Semiconductor Quantum Dots. *Dekker Encyclopedia of Nanoscience and Nanotechnology*. CRC Press, 2nd edition, 2012; appeared on line in September 2012; see http://www.tandfonline.com/doi/pdf/10.1081/E-ENN2-120048425

PRESENTATIONS

Michael A. Stroscio, Mitra Dutta, Sicheng Liao, Banani Sen, Jun Qian, Robin Xu, Nanzhu Zhang, Min Choi, Yi Lan, **Kimber Brenneman**, Xenia Meshik, Preeti Pratap, and Donna Wu, Applications of Physics in Nanoscience and Nanoelectronics. Ball State University, March 28, 2013: Seminar

Kimber L. Brenneman, Shripriya Poduri, Michael A. Stroscio, and Mitra Dutta, Testing Water for Contaminants with a DNA-based Optical Nanosensor. *Society of Women Engineers Annual Conference* 2012. November 9, 2012. Houston, TX: Session Presentation

Kimber L. Brenneman, Katherine Alfredo, Marcella Vaicik, and Prinda Wanakule, Global Opportunities for Graduate Students and Post-Doctorates. *Society of Women Engineers Annual Conference* 2012. Houston, TX: Session Presentation Moderator

Marcella Vaicik, **Kimber L. Brenneman,** and Diane Peters, Returning to Graduate School with Industry Experience. *Society of Women Engineers Webinar*. October 3, 2012, Chicago, IL: Webinar

Kimber L. Brenneman, Xenia Meshik, Ke Xu, Justin Abell, Yiping Zhao, Mitra Dutta, and Michael A. Stroscio, Surface-Enhanced Raman Spectroscopy Study

of Single Stranded DNA Sequences on Silver Nanorod Array. PHONONS 2012, July 8-12, 2012, Ann Arbor, Michigan: Oral Presentation

Ke Xu, Justin Abell, Yiping Zhao, Jun Qian, **Kimber Brenneman**, Xenia Meshik, Mitra Dutta, Michael Stroscio, Surface-Enhanced Raman Spectroscopy as a Tool for Characterizing Nanostructures Containing Molecular Component. PHONONS 2012, July 8-12, 2012, Ann Arbor, Michigan: Poster Presentation

Xenia Meshik, **Kimber Brenneman**, Ke Xu, Justin Abell, Yiping Zhao, Mitra Dutta, Michael Stroscio, Surface-Enhanced Raman Spectroscopy Signatures of an RNA Molecule: An Aptamer that Binds to the αVβ3 Integrin. PHONONS 2012, July 8-12, 2012, Ann Arbor, Michigan: Poster Presentation

Saadia Ranginwala, **Kimber Brenneman**, Xenia Meshik, Justin Abell, Yiping Zhao, Michael Stroscio, and Mitra Dutta, Surface Enhanced Raman Spectroscopy of DNA Aptamer for Immunoglobulin E. PHONONS 2012, July 8-12, 2012, Ann Arbor, Michigan: Poster Presentation

Kimber L. Brenneman, DNA-based nanoconstructs for the detection of heavy metal ions. Oakton Community College Des Plaines, IL October 19, 2011: Seminar Presentation

Kimber L. Brenneman, Banani Sen, Shripriya Poduri, Michael A. Stroscio, and Mitra Dutta, Aptamer-based optical detection of heavy metal ions as a platform for a portable handheld sensing device for environmental monitoring. *Society of Women Engineers Annual Conference 2011.* October 14, 2011. Chicago, IL: Poster Presentation

Shripriya Poduri, **Kimber L. Brenneman**, Michael A. Stroscio, and Mitra Dutta, Aptamer-based optical biosensor for lead (II) ions. *Society of Women Engineers Annual Conference 2011*. October 14, 2011. Chicago, IL: Poster Presentation

Kimber L. Brenneman, Jennifer Patterson, Marcella Vaicik, and Katherine Alfredo, Global Opportunities for Graduate Students and Post-Doctorates. *Society of Women Engineers Annual Conference* 2011. Chicago, IL: Session Presentation Moderator

Kimber L. Brenneman, Olga Shebanova, Kristi Tanouye, and Rebecca MacDonald, Entering Industry with a Graduate Degree. *Society of Women Engineers Annual Conference* 2011. Chicago, IL: Session Presentation Moderator

Marcella Vaicik, **Kimber L. Brenneman,** Anne Lucietto, Diane Peters, Chelsea Spier, Transitioning from Industry to Graduate School. *Society of Women Engineers Annual Conference* 2011. Chicago, IL: Session Presentation Panelist

Kimber L. Brenneman, Banani Sen, Shripriya Poduri, Michael A. Stroscio, and Mitra Dutta, Aptamer-based optical detection of heavy metal ions as a platform for a portable handheld sensing device for environmental monitoring. *Air Force Medical Service Medical Research Symposium,* August 2, 2011. National Harbor, MD: Poster Presentation

Kimber L. Brenneman, Banani Sen, Michael A. Stroscio, and Mitra Dutta, Aptamer-based optical bionano sensor for mercury (II) ions. *IEEE Nanotechnology Materials and Devices Conference,* October 13, 2010. Monterey, CA: Session Presentation

Marcella Schmidt and **Kimber L. Brenneman,** Back to School. *Society of Women Engineers Annual Conference* 2010. Orlando, FL: Session Presentation

Kimber L. Brenneman, Tsai-Chin Wu, Milana Vasudev, Michael A. Stroscio, and Mitra Dutta, Integrated nanostructure-semiconductor-molecular complexes as tools for THz spectral studies of DNA. *International Symposium on Spectral Science Research* 2010. Springfield, MO: Session Presentation

Tsai-Chin Wu, **Kimber L. Brenneman**, Michael A. Stroscio, and Mitra Dutta, Self-administered diagnostic tests to measure physiological indicators using DNA-based nanostructure-semiconductor-molecular complexes. *International Symposium on Spectral Science Research* 2010. Springfield, MO: Session Presentation

SERVICE, AWARDS, and SOCIETY AFFILIATIONS

- Society of Women Engineers (SWE) – Volunteer Abstract Reviewer for WE13 Rapid Fire Graduate Student Research Session, 2013
- Graduate Student Council Travel Award, 2012
- SWE – Graduate Student Task Force member, 2012
- Association for Women in Science (AWIS) – Member, 2010 - Present
- UIC Women in Science and Engineering (WISE) Travel Grant award, December 2010
- Science Fair Judge – Murray Language Academy, December 2010 and 2011
- Society of Women Engineers – Graduate Student Programs committee member, 2010 - present
- Society of Women Engineers – Outreach committee member, 2009
    - Engineer Your Life College Fair Booth Volunteer – October 3, 2009
    - LabFest Volunteer - August 21, 2009
- UIC WISE Women in Nanotechnology (WIN) Mentor, 2009 - present
    - Presented research to visiting high school WISE club, March 16, 2012
    - Presented research at Oakton Community College, October 19, 2011
    - Presented research and provided lab tour to group of prospective students, March 18, 2011
    - Futures Unlimited Conference - Co-presented hands-on workshops for 8th grade girls at Oakton Community College in Skokie, IL

utilizing nanotechnology consumer products with support from the National Girls Collaborative Project Mini-Grant Program, May 20, 2010

  - Co-presented at WIN club event at College of DuPage, September 25, 2009

- Board of Trustees Tuition & Fee Waiver Award – Spring 2009
- Professional Experience Program Internship Award - 2003
- Purdue University Semester Honors – Fall 2003, Fall 1998
- Purdue University Dean's List – Fall 1998